Electronic Transactions on Numerical Analysis.
Volume 63, pp. 368–400, 2025.

ISSN 1068–9613.
DOI: 10.1553/etna_vol63s368

ETNA
Kent State University and
Johann Radon Institute (RICAM)

A COLLOCATION METHOD FOR A NONLOCAL TUMOR GROWTH MODEL*

YASSINE MELOUANI†‡, ABDERRAHMAN BOUAHAMIDI†, AND IMAD EL HARRAKI‡

Abstract. This paper presents a model for tumor growth using a nonlocal velocity. We establish some results on the existence and uniqueness of solutions for a nonlocal tumor growth model. Many experiments show that the tumor spheroid can be invariant under rotation and can maintain the shape of a spheroid during the growth process in some particular cases. Here, we assume that the multiple components of the system are invariant under rotation. Then, we use the collocation method to solve the nonlocal system. To illustrate the efficiency of the proposed method, we performed numerical tests that simulate a tumor growth scenario.

Key words. collocation method, nonlocal tumor growth model, partial differential equations

AMS subject classifications. 35R09, 65M70, 92C50, 35Q92

1. Introduction.

Mathematical modeling of tumor growth has emerged as a critical tool for understanding cancer progression and optimizing therapeutic strategies. Traditional approaches based on local partial differential equations (PDEs) have provided valuable insights into tumor dynamics, yet they face fundamental limitations in capturing the complex multi-scale interactions that characterize malignant growth [3, 28]. Recent advances in biological understanding have revealed that cancer cells communicate and coordinate their behavior through long-range mechanisms that extend far beyond immediate cellular neighborhoods, necessitating a shift toward nonlocal mathematical formulations.

The biological foundation for nonlocal tumor modeling rests on compelling experimental evidence demonstrating direct cell-to-cell communication across multiple cell diameters. Tunneling nanotubes (TNTs), discovered through advanced microscopy techniques, represent thin membranous conduits (50–1000 nm diameter, extending up to 500 μm) that directly connect cancer cells and facilitate the transfer of organelles, proteins, and signaling molecules [31, 32]. Similarly, cytonemes—actin-based membrane protrusions extending up to 100 μm between cells—enable direct protein transport through specialized synaptic contacts [11]. These experimental observations naturally lead to mathematical formulations where velocity terms depend on nonlocal information, reflecting the observed long-range cellular communication.

The mathematical framework for nonlocal tumor growth modeling was established by Armstrong, Painter, and Sherratt [2] in their ground-breaking work introducing integro-partial differential equations (integro-PDEs) that successfully replicated adhesion-driven cell-sorting experiments. The fundamental nonlocal formulation incorporates distributed adhesive forces through integral terms of the form

$$\frac{\partial u}{\partial t} = \nabla \cdot \left(D \nabla u - u \int_{\Omega} K(x,y) g(u(y,t))\, dy \right),$$

where the nonlocal integral term represents cell sensing and interaction mechanisms over finite ranges defined by the kernel function $K(x,y)$ [9, 21].

*Received July 7, 2025. Accepted August 18, 2025. Published online on September 23, 2025. Recommended by Lothar Reichel.

‡Corresponding author: Y. Melouani. Laboratoire de Mathématiques Pures et Appliquées (LMPA), Université du Littoral Côte d'Opale, 62100 Calais, France
({yassine.melouani,abderrahman.bouhamidi}@univ-littoral.fr).

†Laboratoire de Mathématiques Appliquées et d'Informatique Décisionnelle (LMAID), Ecole Nationale Supérieure des Mines, 10000 Rabat, Morocco
({yassine.melouani,elharraki}@enim.ac.ma).

ETNA
Kent State University and
Johann Radon Institute (RICAM)

The mathematical advantages of nonlocal formulations over classical local approaches have become increasingly apparent through theoretical analysis and computational studies. Unlike local models that rely on pointwise gradient information, nonlocal systems naturally accommodate finite-range cellular sensing through mathematically well-posed integral kernels, enabling a more realistic representation of biological interaction ranges [9, 21]. The integro-differential structure inherent in nonlocal models generates substantially richer pattern formation capabilities, supporting complex spatial organizations and bifurcation phenomena that remain inaccessible to local diffusion–reaction systems [4, 11, 23]. Furthermore, nonlocal formulations demonstrate enhanced numerical stability and superior handling of boundary conditions due to the regularizing effects of spatial averaging, which effectively incorporates memory effects that smooth discontinuities and reduce the influence of artificial boundaries [13, 14].

Contemporary research has witnessed significant advances in nonlocal tumor modeling across multiple fronts. Collective migration frameworks have evolved to incorporate experimentally validated coordination mechanisms, leading to more accurate representations of metastatic invasion patterns observed in clinical settings [16, 20, 33, 35]. Patient-specific modeling approaches now integrate advanced imaging modalities with biomechanistic nonlocal models to enable personalized tumor growth predictions, representing a convergence of mathematical sophistication with clinical applicability [28]. These developments have established nonlocal mathematical frameworks as increasingly essential tools for precision oncology applications, where capturing long-range cellular interactions proves critical for accurate treatment planning and outcome prediction [15].

However, the practical implementation of nonlocal tumor models faces significant computational challenges. The integro-differential nature of these equations introduces $O(N^2)$ computational complexity due to the nonlocal integral terms, requiring specialized numerical methods for their efficient solution [13, 22]. Classical finite-difference and finite-element approaches often struggle with the accuracy and stability requirements of nonlocal formulations, particularly when dealing with the stiff systems that commonly arise in biological applications [14].

Current numerical approaches for nonlocal equations include various spectral methods, finite-element techniques, and specialized quadrature schemes [36]. B-spline collocation methods have shown particular promise for fractional integro-differential equations due to their inherent smoothness and flexibility in capturing memory effects [1]. However, the temporal discretization of stiff nonlocal systems remains challenging, with explicit methods requiring impractically small time steps for stability.

Backward differentiation formula (BDF) methods have proven highly effective for solving stiff ordinary differential equation (ODE) systems arising from the spatial discretization of PDEs [18]. For nonlocal tumor growth models, which typically exhibit stiffness due to the coupling between cell populations, nutrient concentrations, and growth factors, implicit methods like BDF offer superior stability properties that enable larger time steps while maintaining accuracy.

In this paper, we use a collocation method based on BDF B-spline techniques to solve the nonlocal tumor growth model. In this model, we consider a three-component system incorporating tumor cell density, healthy cell density, and nutrient concentration, with nonlocal velocity terms that capture cell-cell adhesion and communication mechanisms. Under the assumption of spherical symmetry—which is appropriate for the early-stage avascular tumors and tumor spheroids commonly used in experimental studies [29]—we derive a radial formulation that significantly reduces computational complexity while preserving the essential nonlocal characteristics.

ETNA
Kent State University and
Johann Radon Institute (RICAM)

Our approach combines cubic B-spline spatial discretization with higher-order BDF temporal integration, specifically employing the sixth-order BDF for maximum stability and efficiency. The resulting numerical scheme is validated through a convergence analysis using constructed analytical solutions.

The remainder of this paper is organized as follows. Section 2 presents the nonlocal continuum model. Section 3 establishes theoretical results on the existence and uniqueness of solutions. Section 4 derives the radial formulation under the assumptions of spherical symmetry. Section 5 develops the BDF B-spline numerical method and analyzes its properties. Section 6 presents numerical experiments demonstrating convergence and applicability to tumor growth scenarios. Finally, the last section concludes with discussion and future research directions.

2. A nonlocal continuum model for tumor growth. We develop a nonlocal continuum model that extends classical tumor growth formulations by incorporating experimentally observed long-range cellular interactions. Our approach builds upon the foundational work of Lefebvre et al. [27] while introducing specific nonlocal mechanisms motivated by recent discoveries in cancer cell communication.

Classical tumor growth models typically employ local PDEs where the tumor cell density P evolves according to

$$\frac{\partial P}{\partial t} + \nabla \cdot (v_{\text{local}} P) = \text{Growth} - \text{Death},$$

with velocity fields v_{local} determined by local gradients, such as pressure or nutrient concentration gradients, via Darcy's law. While this formulation has provided valuable insights into tumor dynamics, recent experimental evidence reveals fundamental biological mechanisms that cannot be captured by purely local interactions.

The most compelling evidence comes from the discovery of tunneling nanotube networks in cancer systems. These thin membranous structures, ranging from 50 to 1000 nm in diameter and extending up to 500 μm in length, form direct physical connections between cancer cells separated by distances far exceeding the typical cell dimensions [31, 32]. Through these conduits, cells coordinate their migration decisions based on information from distant cellular states, enabling an organized collective behavior that local models fundamentally cannot represent.

To capture these long-range interactions mathematically, we propose a nonlocal velocity formulation where cells at position x respond to the weighted distribution of tumor cells throughout their sensing neighborhood. We assume that the domain of study is large enough such that there is no interaction between tumor cells and the boundary, and, without loss of generality, we consider the domain as the open disk centered at 0 with radius $R > 0$, denoted as $\Omega_R = \{x \in \mathbb{R}^d : \|x\|_2 < R\}$, where $\|\cdot\|_2$ is the usual Euclidean norm in $\mathbb{R}^d$, and we let $\partial\Omega_R$ be the boundary of Ω_R. The nonlocal velocity is then defined as

$$V[\vec{\alpha}_p, \gamma_p, P](t,x) = \vec{\alpha}_p(t,x) \int_{\Omega_R} \gamma_p(x-y) P(t,y)\, dy,$$

where the directional response function $\vec{\alpha}_p(t,x)$ determines how cells at position x convert sensed signals into directed motion, potentially varying with local conditions such as nutrient availability or mechanical constraints. The sensing kernel γ_p models the decay of cell-cell communication effectiveness with spatial separation, reflecting the finite range and intensity of biological signaling mechanisms. The integral $\int_{\Omega_R} \gamma_p(x-y)P(t,y)\, dy$ represents the nonlocal density field experienced by cells at position x, computed as a weighted average of tumor cell densities throughout their sensing neighborhood.

ETNA
Kent State University and
Johann Radon Institute (RICAM)

This mathematical structure directly reflects that tumor cells integrate information from their surroundings to make movement decisions. Rather than responding only to immediate local gradients, cells process signals from extended neighborhoods, weighting distant information according to the strength and range of their communication mechanisms.

For the sensing kernel, we adopt Gaussian functions as in [5, 15, 16]. Our three-component system models the coupled evolution of the proliferating tumor cells P, the healthy tissue cells S, and the nutrient-oxygen concentration M. To ensure that the growth process remains within the computational domain and there is no interference with the boundary, we introduce a cutoff function $m : \mathbb{R}^d \to \mathbb{R}$ that is infinitely differentiable and satisfies $m(x) = 1$ if $\|x\|_2 \leq R'$ and $m(x) = 0$ if $\|x\|_2 \geq R$, where $R' > 0$ with $R' < R$. This cutoff function ensures that cellular proliferation remains within Ω_R, preventing artificial boundary effects from influencing the biological dynamics. The resulting integro-differential system becomes

$$\begin{aligned}
\frac{\partial P}{\partial t} + \nabla \cdot (V[\vec{\alpha}_p, \gamma_p, P] \cdot P) &= m(x)\,[H(M) - a_1 \lambda(t) M]\,P, \\
\frac{\partial S}{\partial t} + \nabla \cdot (V[\vec{\alpha}_s, \gamma_s, S] \cdot S) &= -a_2 m(x) \lambda(t) M S, \\
\frac{\partial M}{\partial t} - D\,\Delta M &= M_s S(1 - M) - \eta M P,
\end{aligned}$$

subject to the appropriate boundary and initial conditions

$$\begin{aligned}
&P(t,x) = 0, && S(t,x) = S_R, && M(t,x) = M_R, && (t,x) \in [0,T] \times \partial\Omega_R, \\
&P(0,x) = P_0(x), && S(0,x) = S_0(x), && M(0,x) = M_0(x), && x \in \Omega_R.
\end{aligned}$$

The growth dynamics is governed by the sigmoid function

$$H(M) = \kappa\,\frac{1 + \tanh(\delta(M - M_{\text{threshold}}))}{2},$$

which captures the transition between proliferative and hypoxic regimes as nutrient levels cross the critical threshold $M_{\text{threshold}}$. This formulation, adopted from Lefebvre et al. [27], provides a smooth mathematical representation of the sharp biological switch between the growth and quiescence observed in tumor spheroids and clinical tumors.

Treatment effects enter through the drug concentration term $\lambda(t)$, where a_1 represents the tumor cell resistance to therapy and a_2 quantifies the treatment toxicity to healthy tissue. The nutrient dynamics follow a classical reaction–diffusion behavior, with healthy cells producing nutrients at rate M_s subject to carrying capacity limitations $(1 - M)$, while tumor cells consume nutrients at rate η proportional to their local density and nutrient availability.

Since the solution is compactly supported within the computational domain, we restrict the convolution terms by integrating only over Ω_R, which leads us to express the nonlocal velocities as

$$\begin{aligned}
V[\vec{\alpha}_p, \gamma_p, P](t,x) &= \vec{\alpha}_p(t,x) \int_{\Omega_R} \gamma_p(x - y) P(t,y)\,dy, \\
V[\vec{\alpha}_s, \gamma_s, S](t,x) &= \vec{\alpha}_s(t,x) \int_{\Omega_R} \gamma_s(x - y) S(t,y)\,dy.
\end{aligned}$$

ETNA
Kent State University and
Johann Radon Institute (RICAM)

Regrouping the equations with their boundary conditions, the complete system becomes

$$
\text{(2.1)}\qquad
\begin{cases}
\dfrac{\partial P}{\partial t}(t,x) + \nabla \cdot \big[V[\vec{\alpha}_p, \gamma_p, P](t,x)P(t,x)\big] \\
\qquad = m(x)\big(H(M(t,x))P(t,x) - a_1\lambda(t)M(t,x)P(t,x)\big), \\
\dfrac{\partial S}{\partial t}(t,x) + \nabla \cdot \big[V[\vec{\alpha}_s, \gamma_s, S](t,x)S(t,x)\big] = -a_2 m(x)\lambda(t)M(t,x)S(t,x), \\
\dfrac{\partial M}{\partial t}(t,x) - D\Delta M(t,x) = M_s S(t,x)(1 - M(t,x)) - \eta M(t,x)P(t,x), \\
P(t,x) = 0, \quad S(t,x) = S_R, \quad M(t,x) = M_R, \quad (t,x) \in [0,T] \times \partial\Omega_R, \\
P(0,x) = P_0(x), \quad S(0,x) = S_0(x), \quad M(0,x) = M_0(x), \quad x \in \Omega_R.
\end{cases}
$$

Letting $U = (P, S, M)$, we rewrite the system of equations (2.1) in the following form:

$$
\text{(2.2)}\qquad
\begin{cases}
\dfrac{\partial U}{\partial t}(t,x) + \mathcal{A}(U)(t,x) = G(U)(t,x), & (t,x) \in [0,T] \times \Omega_R, \\
U(t,x) = U_R, & (t,x) \in [0,T] \times \partial\Omega_R, \\
U(0,x) = U_0(x), & x \in \Omega_R,
\end{cases}
$$

with

$$
\mathcal{A}(U)(t,x) = \left[\nabla \cdot \left(\vec{\alpha}_p(t,x) \int_{\Omega_R} \gamma_p(x-y)P(t,y)\,dy \cdot P(t,x)\right),\right.
$$
$$
\left.\nabla \cdot \left(\vec{\alpha}_s(t,x) \int_{\Omega_R} \gamma_s(x-y)S(t,y)\,dy \cdot S(t,x)\right),\ -D\Delta M\right],
$$
$$
G(U) = \begin{bmatrix} g_1(U) \\ g_2(U) \\ g_3(U) \end{bmatrix} = \begin{bmatrix} mP(H(M) - a_1\lambda M) \\ -ma_2\lambda MS \\ M_s S(1-M) - \eta MP \end{bmatrix},
$$
$$
U_R = (0, S_R, M_R), \quad \text{and} \quad U_0 = (P_0, S_0, M_0).
$$

3. Existence and uniqueness of solution. Our aim in this section is to prove the existence and uniqueness of solutions for the system outlined in equation (2.1). We begin by examining the local dynamics through the isolation of the convolution term and using established principles from the theory of semilinear evolution equations. Following this, we integrate insights from the theory of nonlocal balance equations, as elaborated in [24] and [25], to affirm the existence and uniqueness of solutions for the system mentioned in equation (2.2).

Before proceeding with the existence and uniqueness proofs, we need to define the following spaces. Let $L^\infty(\Omega_R)$ be the space of essentially bounded measurable functions on Ω_R, equipped with the norm

$$
\|f\|_{L^\infty(\Omega_R)} = \operatorname*{ess\,sup}_{x \in \Omega_R} |f(x)|.
$$

Let $C(\Omega_R)$ be the space of continuous functions on Ω_R with the uniform norm

$$
\|f\|_{C(\Omega_R)} = \sup_{x \in \Omega_R} |f(x)|.
$$

ETNA
Kent State University and
Johann Radon Institute (RICAM)

Let $C_b^1(\Omega_R)$ be the space of continuously differentiable functions on Ω_R with bounded derivatives, normed by

$$\|f\|_{C_b^1(\Omega_R)} = \|f\|_{C(\Omega_R)} + \|\nabla f\|_{C(\Omega_R)}.$$

For a Banach space $(X, \|\cdot\|_X)$, let $C([0,T];X)$ denote the space of continuous functions from $[0,T]$ to X with the norm

$$\|f\|_{C([0,T];X)} = \sup_{t\in[0,T]} \|f(t)\|_X.$$

Let $L^1([0,T];X)$ be the space of Bochner-integrable functions from $[0,T]$ to X with the norm

$$\|f\|_{L^1([0,T];X)} = \int_0^T \|f(t)\|_X \, dt.$$

Let $W^{2,1}(\Omega_R)$ be the Sobolev space defined as

$$W^{2,1}(\Omega_R) = \{u \in L^1(\Omega_R) : D^\alpha u \in L^1(\Omega_R) \text{ for all } |\alpha| \le 2\}.$$

3.1. Existence and uniqueness of the solution of the local system. Let w_p and w_s be two fixed functions belonging to $C([0,T], C_b^1(\mathbb{R}^d))$, and let $w := (w_p, w_s)$. We consider the associated local system to (2.2), written as follows:

$$\text{(3.1)} \qquad \begin{cases} \dfrac{\partial U_w}{\partial t}(t,x) + \mathcal{A}_w(U_w)(t,x) = G(U_w)(t,x), & (t,x) \in [0,T]\times\Omega_R, \\ U_w(t,x) = U_R, & (t,x) \in [0,T]\times\partial\Omega_R, \\ U(0,x) = U_0(x), & x \in \Omega_R, \end{cases}$$

with $\mathcal{A}_w(U) = \big[\nabla\cdot(\vec{\alpha}_p(t,x)w_p(t,x)P_w(t,x)),\ \nabla\cdot(\vec{\alpha}_s(t,x)w_s(t,x)S_w(t,x)),\ -D\Delta M\big]$, and

$$G(U_w) = \begin{bmatrix} g_1(U_w) \\ g_2(U_w) \\ g_3(U_w) \end{bmatrix} = \begin{bmatrix} mP_w(H(M_w) - a_1\lambda M_w) \\ -ma_2\lambda M_w S_w \\ M_s S_w(1-M_w) - \eta M_w P_w \end{bmatrix},$$

and we have $U_R = (0, S_R, M_R)$ and $U_0 = (P_0, S_0, M_0)$.

To ensure that the solution remains positive and bounded within the domain, we make the following assumptions regarding initial conditions and velocities:

ASSUMPTION 3.1. *We assume that*

(A1) $U_0 \in C^1(\Omega_R)^3 := C^1(\Omega_R)\times C^1(\Omega_R)\times C^1(\Omega_R)$,
(A2) $U_0 = (P_0, S_0, M_0) \ge 0$, *which means* $P_0 \ge 0$, $S_0 \ge 0$, *and* $M_0 \ge 0$,
(A3) $U_0 - U_R$ *is compactly supported in* Ω_R,
(A4) $\vec{\alpha}_k \in C^2([0,T]\times\Omega_R;\mathbb{R}^d)$, $k = p, s$,
(A5) $\vec{\alpha}_s$ *is compactly supported in* $[0,T]\times\Omega_R$, *and*
(A6) $\lambda \in C([0,T])$.

The Banach space $L^\infty(\Omega_R)^3 := L^\infty(\Omega_R)\times L^\infty(\Omega_R)\times L^\infty(\Omega_R)$ is equipped here with the norm

$$\|f\|_{L^\infty(\Omega_R)^3} = \|f_1(t)\|_{L^\infty(\Omega_R)} + \|f_2(t)\|_{L^\infty(\Omega_R)} + \|f_3(t)\|_{L^\infty(\Omega_R)} \quad \text{for all} \quad f = (f_1, f_2, f_3) \in L^\infty(\Omega_R)^3.$$

ETNA
Kent State University and
Johann Radon Institute (RICAM)

THEOREM 3.2. *Let the assumptions (A1)–(A6) hold. Then there exists a maximal time $T_{\max}$ such that equation (3.1) has a unique positive solution in $C([0,T],L^\infty(\Omega_R)^3)$. Furthermore, $U(t,\cdot)_w - U_R$ is a compactly supported function in Ω_R for all $t \le T_{\max}$.*

Proof. To establish existence and uniqueness for (3.1), we apply the characteristic method. First, we ensure that there is no interaction between the tumor and the boundary by selecting T so that the characteristics are appropriately defined within Ω_R. This is guaranteed by the fact that $U_0 - U_R$ and the velocity vectors of healthy cells have a compact support in Ω_R. Let $0 < R_0 < R$ be such that $\operatorname{supp}(U_0) \cup \operatorname{supp}(\vec{\alpha}_p) \subset \Omega_{R_0}$, and let

$$R_i = R_0 + \frac{i(R-R_0)}{3}, \qquad \text{for } i = 1,2,3.$$

In order to prevent the characteristic curves from exiting Ω_R, we proceed under the assumption that $T \le T_{\max}$ is sufficiently small such that

$$T < T_1^* := \frac{R-R_0}{3\max\{\|\vec{\alpha}_p w_p\|_{C([0,T_{\max}],L^\infty(\Omega_R))},\ \|\vec{\alpha}_s w_s\|_{C([0,T_{\max}],L^\infty(\Omega_R))}\}}$$

with $T_{\max}$ a large fixed value. The characteristics are well defined for all $t,s \in [0,T]$ and $x \in \Omega_{R_2}$ as follows:

$$\begin{aligned}\frac{\partial X[t,x]_{w_p}(s)}{\partial s} &= \vec{\alpha}_p(s, X[t,x]_{w_p}(s))\, w_p(s, X[t,x]_{w_p}(s)),\\ X[t,x]_{w_p}(t) &= x,\end{aligned}$$

and

$$\begin{aligned}\frac{\partial X[t,x]_{w_s}(s)}{\partial s} &= \vec{\alpha}_s(s, X[t,x]_{w_s}(s))\, w_s(s, X[t,x]_{w_s}(s)),\\ X[t,x]_{w_s}(t) &= x.\end{aligned}$$

In fact, let $x \in \Omega_{R_2}$. By using the condition on the final time T, we have for $k = p, s$

$$\begin{aligned}\|X[t,x]_{w_k}(s)\|_2 &\le \|x\|_2 + \|X[t,x]_{w_k}(s) - x\|_2\\ &\le R_2 + \int_t^s \|\vec{\alpha}_k(s, X[t,x]_{w_k}(s))\, w_k(s, X[t,x]_{w_k}(s))\|_2\, ds\\ &\le R_0 + \tfrac{2}{3}(R-R_0) + T\|\vec{\alpha}_k w_k\|_{C([0,T],L^\infty(\Omega_R))}\\ &< R_0 + \tfrac{2}{3}(R-R_0) + \tfrac{1}{3}(R-R_0) = R.\end{aligned}$$

For $(t,x) \in [0,T] \times \Omega_{R_2}$, using the semi-explicit form for the local balance law in [25], we have

$$\begin{aligned}P_w(t,x) &= P_0(X[t,x]_{w_p}(0))\det(DX[t,x]_{w_p}(0))\\ &\quad + \int_0^T \det(DX[t,x]_{w_p}(s))\, g_1(U_w)(s, X[t,x]_{w_p}(s))\, ds\\ S_w(t,x) &= S_0(X[t,x]_{w_s}(0))\det(DX[t,x]_{w_s}(0))\\ &\quad + \int_0^T \det(DX[t,x]_{w_s}(s'))\, g_2(U_w)(s', X[t,x]_{w_s}(s'))\, ds',\end{aligned}$$

ETNA
Kent State University and
Johann Radon Institute (RICAM)

with

$$\det(DX[t,x]_{w_k}(s)) = \exp\left(\int_t^s \operatorname{div}\big(\vec{\alpha}_k(s, X[t,x]_{w_k}(s))\, w_k(s, X[t,x]_{w_k}(s))\big)\, ds\right) \tag{3.2}$$

for $k = p, s$. Now, letting $t, s \in [0,T]$ and $x \in \Omega_{R_2} \setminus \Omega_{R_1}$, we then have

$$\begin{aligned} \|X[t,x]_{w_k}(s)\|_2 &\geq \big|\, \|x\|_2 - \|X[t,x]_{w_k}(s) - x\|_2 \,\big| \qquad (\text{for } k = p, s) \\ &> \big|R_1 - \tfrac{1}{3}(R - R_0)\big| = R_0. \end{aligned}$$

Using the assumption that initial functions are compactly supported in Ω_{R_0}, we deduce that $P_0(X[t,x]_{w_p}(0)) = 0$ and $S_0(X[t,x]_{w_s}(0)) = S_R$. Furthermore, the function m ensures that the right-hand side is compactly supported in Ω_R by choosing $R' \leq R_0$. Using the assumption of the compactness of the support of $\vec{\alpha}_s$, we get $P_w(t,x) = 0$ and $S_w(t,x) = S_R$ for all $(t,x) \in [0,T] \times \Omega_{R_2} \setminus \Omega_{R_1}$. Using equation (3.1), we can smoothly extend P and S to be constant in $\Omega_R \setminus \Omega_{R_2}$.

The equation of nutrients M is a semilinear parabolic equation; therefore, by using the maximum principle, we deduce that $U_w - U_R$ is compactly supported in Ω_R.

Now we prove local existence and uniqueness for equation (3.1). To do this, we employ a classical approach for semilinear evolutionary equations using Banach's fixed-point theorem. This approach has been demonstrated in works such as [10, 37].

In the first step, we show that the right-hand side is locally Lipschitzian. In fact, let $L > 0$ for $U_w = (P_w, S_w, M_w)$ and $V_w = (P'_w, S'_w, M'_w)$ in $C([0,T], L^\infty(\Omega_R)^3)$ such that $\|U_w\|_{C([0,T],L^\infty(\Omega_R)^3)}, \|V_w\|_{C([0,T],L^\infty(\Omega_R)^3)} \leq L$. Then we have

$$\begin{aligned} &\|G(U_w(t)) - G(V_w(t))(t)\|_{L^\infty(\Omega_R)^3} \\ &\quad = \|g_1(U_w(t)) - g_1(V_w(t))\|_\infty + \|g_2(U_w(t)) - g_2(V_w(t))\|_\infty \\ &\qquad + \|g_3(U_w(t)) - g_3(V_w(t))\|_\infty. \end{aligned}$$

By using the fact that $\|H(M)\|_{C([0,T],L^\infty(\Omega_R))} \leq \kappa$ together with the inequalities

$$\begin{aligned} \|g_1(U_w(t)) - g_1(V_w(t))\|_\infty &\leq \kappa \|P_w(t) - P'_w(t)\|_\infty \\ &\quad + a_1 L\big(\|P_w(t) - P'_w(t)\|_\infty + \|M_w(t) - M'_w(t)\|_\infty\big), \end{aligned}$$

$$\begin{aligned} \|g_2(U_w(t)) - g_2(V_w(t))\|_\infty &\leq a_2 L\big(\|S_w(t) - S'_w(t)\|_\infty + \|M_w(t) - M'_w(t)\|_\infty\big) \\ &\quad + M_s M_R \|S_w(t) - S'_w(t)\|_\infty, \end{aligned}$$

and

$$\begin{aligned} \|g_3(U_w(t)) - g_3(V_w(t))\|_\infty &\leq M_s L\big(\|S_w(t) - S'_w(t)\|_\infty + \|M_w(t) - M'_w(t)\|_\infty\big) \\ &\quad + \eta L\big(\|P_w(t) - P'_w(t)\|_\infty + \|M_w(t) - M'_w(t)\|_\infty\big), \end{aligned}$$

we get

$$\|G(U_w(t)) - G(V_w(t))\|_{L^\infty(\Omega_R)^3} \leq C(L)\|U_w(t) - V_w(t)\|_\infty,$$

where $C(L)$ is a positive function depending on the constant L. Finally, by taking the maximum over the time $t \in [0,T]$, we get the result.

For the next step, we consider the following constants:

$$C_k = \|\vec{\alpha}_k\|_\infty \|\nabla w_k\|_\infty + \|\nabla \cdot (\vec{\alpha}_k)\|_\infty \|w_k\|_\infty \quad \text{and} \quad C_v = e^{T \max\{C_p, C_s\}} \geq 1. \tag{3.3}$$

ETNA
Kent State University and
Johann Radon Institute (RICAM)

Let $K = 2LC_v$. We denote the closed ball of radius K (closed convex) of the Banach space $C([0,T], L^\infty(\Omega_R)^3)$ by

$$E = \{f \in C([0,T], L^\infty(\Omega_R)^3) : \|f\|_{C([0,T],L^\infty(\Omega_R)^3)} \le K\}.$$

Letting $U_w \in E$, we consider the following functional:

$$\Phi(U_w)(t) = \begin{bmatrix} P_0(X[t,x]_{w_p}(0)) \det(DX[t,x]_{w_p}(0)) \\ \quad + \displaystyle\int_0^T \det(DX[t,x]_{w_p}(s))\, g_1(U_w)(s, X[t,x]_{w_p}(s))\, ds \\ S_0(X[t,x]_{w_s}(0)) \det(DX[t,x]_{w_s}(0)) \\ + \displaystyle\int_0^T \det(DX[t,x]_{w_s}(s'))\, g_2(U_w)(s', X[t,x]_{w_s}(s'))\, ds' \\ \mathcal{T}(t)M_0 + \displaystyle\int_0^T \mathcal{T}(t-s) g_2(U_w)(s)\, ds \end{bmatrix},$$

where $t \to \mathcal{T}(t)$ is the semigroup of the heat operator $A = -D\Delta$ with domain

$$D(A) = \{u \in W^{2,1}(\Omega_R) : Au \in L^\infty(\Omega_R),\ u|_{\partial\Omega_R} = M_R\}.$$

The semigroup $t \to \mathcal{T}(t)$ satisfies

$$\|\mathcal{T}(t)M_0\|_{C([0,T],L^\infty(\Omega_R))} \le \|M_0\|_{L^\infty(\Omega_R)} \qquad \text{for all } t \in [0,T] \tag{3.4}$$

(see [6] for more details).

First, let us show that $\Phi(E) \subseteq E$. Let $U_w \in E$; we have

$$\begin{aligned} \|\Phi(U_w)(t)\|_\infty = &\Big\| P_0(X[t,x]_{w_p}(0)) \det(DX[t,x]_{w_p}(0)) \\ &\quad + \int_0^T \det(DX[t,x]_{w_p}(s))\, g_1(U_w)(s, X[t,x]_{w_p}(s))\, ds \Big\|_\infty \\ &+ \Big\| S_0(X[t,x]_{w_s}(0)) \det(DX[t,x]_{w_s}(0)) \\ &\quad + \int_0^T \det(DX[t,x]_{w_s}(s'))\, g_2(U_w)(s', X[t,x]_{w_s}(s'))\, ds' \Big\|_\infty \\ &+ \Big\| \mathcal{T}(t)M_0 + \int_0^T \mathcal{T}(t-s)\, g_3(U_w)(s)\, ds \Big\|_\infty . \end{aligned}$$

By using (3.2), (3.3), and (3.4), and the estimates from [25], we obtain

$$\|\det(DX[t,x]_{w_k}(s))\|_{C([0,T],L^\infty(\Omega_R))} \le C_v \qquad (\text{for } k = p, s).$$

Then, it follows that

$$\begin{aligned} \|\Phi(U_w)(t)\|_\infty \le\ & C_v(\|P_0\|_\infty + \|S_0\|_\infty) + \|M_0\|_\infty \\ & + T\big[C_v\big(\|g_1(U_w)(t)\|_\infty + \|g_2(U_w)(t)\|_\infty\big) + \|g_3(U_w)(t)\|_\infty\big]. \end{aligned}$$

ETNA
Kent State University and
Johann Radon Institute (RICAM)

Using the Lipschitz property of G and $G(0) = 0$, we have

$$\begin{aligned}\|\Phi(U_w)(t)\|_\infty &\le C_v\Big[(\|P_0\|_\infty + \|S_0\|_\infty + \|M_0\|_\infty)\\ &\qquad + TC(L)\big(\|g_1(U_w)(t)\|_\infty + \|g_2(U_w)(t)\|_\infty + \|g_3(U_w(t))\|_\infty\big)\Big]\\ &\le C_v L(1 + TC(L)).\end{aligned}$$

Then, by choosing

$$T \le T_2^* := \min\left\{T_1^*, \frac{1}{2C(L)}\right\} \tag{3.5}$$

and taking the maximum over time, we deduce that $\Phi(E) \subseteq E$. Now, let $U_w, U_w' \in E$; we have

$$\|\Phi(U_w) - \Phi(U_w')\|_E \le TC_v\|U_w - U_w'\|_E \le \tfrac{1}{2}\|(U_w - U_w'\|_E.$$

Therefore, Φ is a contraction in E with Lipschitz constant $1/2$, and so Φ has a fixed point $U_w \in E$, which ensures the existence and uniqueness of a solution of (3.1). ∎

3.2. Existence and uniqueness of the nonlocal system. Now we turn back to the nonlocal system (2.2). We use Banach's fixed theorem once again as in [25] to obtain the main theorem.

THEOREM 3.3. *Let the assumptions (A1)–(A6) hold, and assume that $\gamma_p, \gamma_s \in C_b^1(\Omega_R)$. Then the system of equations (2.2) has a unique solution $U = (P, S, M)$ in the Banach space $C([0,T], L^\infty(\Omega_R)^3)$.*

Proof. In the proof, we follow the lines of [25] adapted to the case of a system of coupled nonlocal equations.

Let us define the following constants:

$$N_p := \|\gamma_p\|_{C([0,T]\times\Omega_R)}\left(\|P_0\|_{L^1(\Omega_R)} + \sup_{w\in C([0,T],C_b^1(\Omega_R))^2}\|g_1(U_w)\|_{L^1([0,T],L^1(\Omega_R))}\right),$$

$$dN_p := \left\|\frac{d\gamma_p}{dx}\right\|_{C([0,T]\times\Omega_R)}\left(\|P_0\|_{L^1(\Omega_R)} + \sup_{w\in C([0,T],C_b^1(\Omega_R))^2}\|g_1(U_w)\|_{L^1([0,T],L^1(\Omega_R))}\right),$$

and

$$N_s := \|\gamma_s\|_{C([0,T]\times\Omega_R)}\left(\|S_0\|_{L^1(\Omega_R)} + \sup_{w\in C([0,T],C_b^1(\Omega_R))^2}\|g_2(U_w)\|_{L^1([0,T],L^1(\Omega_R))}\right),$$

$$dN_s := \left\|\frac{d\gamma_s}{dx}\right\|_{C([0,T]\times\Omega_R)}\left(\|S_0\|_{L^1(\Omega_R)} + \sup_{w\in C([0,T],C_b^1(\Omega_R))^2}\|g_2(U_w)\|_{L^1([0,T],L^1(\Omega_R))}\right),$$

ETNA
Kent State University and
Johann Radon Institute (RICAM)

where $C([0,T],C_b^1(\Omega_R))^2 := C([0,T],C_b^1(\Omega_R)) \times C([0,T],C_b^1(\Omega_R))$.

REMARK 3.4. We have shown in Theorem 3.2 that, by the compactness of the initial data, the velocities, and the semilinear terms, we have boundedness of the local solution. Therefore $G(U_w) = (g_1(U_w), g_2(U_w), g_3(U_w))$ is bounded for every $w \in C([0,T],C_b^1(\Omega_R))^2$.

We now set $N = \max\{N_p, N_s\}$ and $N_z = \max\{dN_p, dN_s\}$. Then we consider

$$B = \big\{ f \in C([0,T],C_b^1(\Omega_R))^2 \mid \|f\|_{C([0,T],C(\Omega_R))^2} \le N,\ \|\nabla f\|_{C([0,T],C(\Omega_R))^2} \le N_z \big\}.$$

It is known that B is a closed subset of a Banach space. Now we verify that $\mathcal{F}$ is a contraction on B. Let $w := (w_p, w_s) \in B$. We consider the following mapping $\mathcal{F}$:

$$\begin{aligned}\mathcal{F}(w)(t,x) &= \begin{bmatrix} \mathcal{F}_1(w)(t,x) \\ \mathcal{F}_2(w)(t,x) \end{bmatrix} \\ &= \begin{bmatrix} \displaystyle\int_{X_{w_p}[t,\Omega_R](0)} \gamma_p(x - X_{w_p}[0,y](t))\, P_0(y)\, dy \\ \displaystyle + \int_{\Omega_R}\int_0^T \gamma_p(x - X_{w_p}[s,y](t))\, g_1(U_w)(s,y)\, dy\, ds \\ \displaystyle\int_{X_{w_s}[t,\Omega_R](0)} \gamma_s(x - X_{w_s}[0,y](t))\, S_0(y)\, dy \\ \displaystyle + \int_{\Omega_R}\int_0^T \gamma_s(x - X_{w_s}[s',y](t))\, g_2(U_w)(s',y)\, dy\, ds' \end{bmatrix}.\end{aligned}$$

Let us introduce the notation

$$\begin{aligned}\Lambda_1(P,g) &:= \|P\|_{L^1(\Omega_R)} + \sup_{w \in C([0,T],C_b^1(\Omega_R))^2} \|g(U_w)\|_{L^1([0,T],L^1(\Omega_R))}, \\ \Lambda_\infty(P,g) &:= \|P\|_{L^\infty(\Omega_R)} + \sup_{w \in C([0,T],C_b^1(\Omega_R))^2} \|g(U_w)\|_{L^1([0,T],L^\infty(\Omega_R))}, \\ C_\infty(P,g,\gamma) &:= 1 + 8RC_v\|\gamma\|_{C([0,t]\times\Omega_R)}\Lambda_\infty(P,g).\end{aligned}$$

Following the same lines as in [25], we can show that $\mathcal{F}(B) \subset B$, and we have for $w, w' \in B$ the following estimates:

$$\begin{aligned}|\mathcal{F}_1(w)(t,x) - \mathcal{F}_1(w')(t,x)| \le{}& \big\|X_{w_p}[t,\cdot](*) - X_{w_p'}[t,\cdot](*)\big\|_{C([0,t]\times\Omega_R)} \\ &\times \|\gamma_p(t,\cdot)\|_{C_b^1(\Omega_R)}\, \Lambda_1(P_0,g_1)\, C_\infty(P_0,g_1,\gamma_p),\end{aligned}$$

and we also have

$$\begin{aligned}&\big\|X_{w_p}[t,\cdot](*) - X_{w_p'}[t,\cdot](*)\big\|_{C([0,t]\times\Omega_R)} \\ &\quad\le T\|w_p - w_p'\|_{C([0,t];C(\Omega_R))} \exp(T(N_z + \|D\vec{\alpha}_p\|_{L^\infty([0,t]\times\Omega_R)})).\end{aligned}$$

Then we get

$$\begin{aligned}&|\mathcal{F}_1(w)(t,x) - \mathcal{F}_1(w')(t,x)| \\ &\quad\le T\|w_p - w_p'\|_{C([0,t];C(\Omega_R))} \exp(T(N_z + \|D\vec{\alpha}_p\|_{L^\infty([0,t]\Omega_R)})) \\ &\qquad\times \|\gamma_p(t,\cdot)\|_{C_b^1(\Omega_R)}\, \Lambda_1(P_0,g_1)\, C_\infty(P_0,g_1,\gamma_p).\end{aligned} \tag{3.6}$$

ETNA
Kent State University and
Johann Radon Institute (RICAM)

Using the same estimates, we get similarly

$$
\begin{aligned}
(3.7)\qquad & |\mathcal{F}_2(w)(t,x) - \mathcal{F}_2(w')(t,x)| \\
&\le T\|w_s - w'_s\|_{C([0,t];C(\Omega_R))} \exp(T(N_z + \|D\vec{\alpha}_s\|_{L^\infty([0,t]\Omega_R)})) \\
&\qquad \times \|\gamma_s(t,\cdot)\|_{C_b^1(\Omega_R)}\, \Lambda_1(S_0,g_2)\, C_\infty(S_0,g_2,\gamma_s).
\end{aligned}
$$

By summing the two estimates (3.6) and (3.7), we deduce that $\mathcal{F}$ is Lipschitz continuous. Then by choosing T small enough we have

$$
\|\mathcal{F}(w) - \mathcal{F}(w')\|_{C([0,T],C(\Omega_R))^2} < \tfrac{1}{2}\|w - w'\|_{C([0,T],C(\Omega_R))^2}.
$$

Therefore, $\mathcal{F}$ is a contraction on B. Then using Banach's fixed point theorem, there exists a unique fixed point $w \in B$ such that $\mathcal{F}(w) = w$ for $t \le T^*$. Furthermore, [25, Theorem 3.24] ensures that existence and uniqueness of the solution hold also for any final time $T > 0$. Hence, in our case we have existence and uniqueness for all $t \le T_2^*$ given in (3.5). ∎

4. Radial model reformulation. Experiments show that a tumor spheroid can be invariant under rotation and can hold the shape of a spheroid during the growth process in some cases [7, 26, 34]. In this paper, in order to simplify our presented model, we assume that the behaviour of a tumor spheroid holds for all $t \le T$, and we use the assumption of rotational invariance to write the model in radial coordinates, which allows us to obtain a simplified expression of the model.

Let $f : \mathbb{R}^d \to \mathbb{R}$ be a radial function. By definition there exists a function $\widetilde{f}$ that satisfies

$$
f(x) = \widetilde{f}(\|x\|) = \widetilde{f}(r) \qquad \text{for all } x \in \mathbb{R}^d, \text{ with } r = \|x\|.
$$

Under the assumption of invariance under rotation, P is a radial function. We also assume that S, M, $\vec{\alpha_k}$, γ_k, and m are radial for $k = p, s$.

The next proposition is crucial for the characterization of a radial expression for the nonlocal term.

PROPOSITION 4.1 (Convolution of two radial functions). *Let f and g be two radial functions, defined from $\mathbb{R}^d$ to $\mathbb{R}$ such that $f * g$ is well defined. Then the convolution product $f * g$ is also a radial function. Furthermore, we have, for all $x \in \mathbb{R}^d$*

$$
f * g(x) = \widetilde{f * g}(r) = \widetilde{f} \mathbin{\widetilde{*}} \widetilde{g}(r),
$$

where $\widetilde{f} \mathbin{\widetilde{*}} \widetilde{g}$ is defined as

$$
\begin{aligned}
\widetilde{f} \mathbin{\widetilde{*}} \widetilde{g}(r) = {} & \frac{2\pi^{(d-1)/2}}{\Gamma((d-1)/2)} \\
& \times \int_0^{+\infty} \left[\int_0^{\pi} \widetilde{f}\big(\sqrt{s^2 + r^2 + 2rs\cos(\theta)}\,\big) s^{d-1} \sin^{d-2}(\theta)\, d\theta \right] \widetilde{g}(s)\, ds,
\end{aligned}
$$

where Γ denotes the classical Gamma function.

Proof. Let x_1 and x_2 be two vectors in $\mathbb{R}^d$, such that $\|x_1\| = \|x_2\|$. A classical result in linear algebra states that there exists an orthogonal endomorphism A such that $Ax_2 = x_1$. Then we have

$$
f * g(x_1) = \int_{\mathbb{R}^d} f(x_1 - y) g(y)\, dy = \int_{\mathbb{R}^d} f(Ax_2 - y) g(y)\, dy.
$$

ETNA
Kent State University and
Johann Radon Institute (RICAM)

With the substitution $y = Az$, using the fact that $|\det(A)| = 1$, we get

$$f * g(x_1) = \int_{\mathbb{R}^d} f(Ax_2 - Az)g(Az)\,dz.$$

So we have

$$f * g(x_1) = \int_{\mathbb{R}^d} f(A(x_2 - z))g(Az)\,dz = \int_{\mathbb{R}^d} f(x_2 - z)g(z)\,dz = f * g(x_2).$$

This shows that $f * g$ is a radial function. By using the fact that the convolution product $f * g$ is radial, we get

$$\begin{aligned} f * g(x) = f * g(\|x\|e_1) &= \int_{\mathbb{R}^d} f(\|x\|e_1 - y)g(y)\,dy \\ &= \int_{\mathbb{R}^d} \widetilde{f}\big(\big\|\|x\|e_1 - y\big\|\big)\widetilde{g}(\|y\|)\,dy \\ &= \int_{\mathbb{R}^d} \widetilde{f}\Big(\sqrt{(\|x\| - y_1)^2 + \|\tilde{y}\|_2^2}\Big)\,\widetilde{g}\Big(\sqrt{y_1^2 + \|\tilde{y}\|_2^2}\Big)dy, \end{aligned}$$

with $e_1 = (1, 0, \ldots, 0) \in \mathbb{R}^d$ and $\tilde{y} = (y_2, y_3, \ldots, y_d) \in \mathbb{R}^{d-1}$. Using Fubini's theorem, we get the following:

$$f * g(x) = \int_{\mathbb{R}} \left(\int_{\mathbb{R}^{d-1}} \widetilde{f}\Big(\sqrt{(\|x\| - y_1)^2 + \|\tilde{y}\|_2^2}\Big)\,\widetilde{g}\Big(\sqrt{y_1^2 + \|\tilde{y}\|_2^2}\Big)d\tilde{y} \right) dy_1.$$

We recall that, for a radial function h on $\mathbb{R}^d$, we have the formula

$$\int_{\mathbb{R}^d} h(x)\,dx = \omega_d \int_0^{+\infty} \widetilde{h}(r) r^{d-1}\,dr,$$

where $\omega_d = 2\pi^{d/2}/\Gamma(d/2)$ denotes the measure of the unit sphere in $\mathbb{R}^d$. Then, we may write

$$f * g(x) = \omega_{d-1} \int_{\mathbb{R}} \left(\int_0^{+\infty} \widetilde{f}\Big(\sqrt{(\|x\| - y_1)^2 + \tilde{r}^2}\Big)\,\widetilde{g}\Big(\sqrt{y_1^2 + \tilde{r}^2}\Big)\tilde{r}^{d-2}d\tilde{r} \right) dy_1,$$

where $\tilde{r} = \|\tilde{y}\|$ is the 2-norm in $\mathbb{R}^{d-1}$. By using polar coordinates

$$\begin{aligned} \Psi :]0, +\infty[\times]-\pi/2, \pi/2[&\longrightarrow]0, +\infty[\times \mathbb{R} \\ (s, \varphi) &\longmapsto (\tilde{r}(s, \varphi) = s\cos(\varphi),\ y_1(s, \varphi) = s\sin(\varphi)), \end{aligned}$$

we obtain

$$\begin{aligned} f * g(x) &= \omega_{d-1} \int_0^{+\infty} \int_{-\pi/2}^{\pi/2} \widetilde{f}\Big(\sqrt{(\|x\| - s\sin(\varphi))^2 + s^2\cos^2(\varphi)}\Big) \\ &\qquad \times \widetilde{g}(s) s^{d-2} \cos^{d-2}(\varphi) s\,d\varphi\,ds \\ &= \omega_{d-1} \int_0^{+\infty} \int_{-\pi/2}^{\pi/2} \widetilde{f}\Big(\sqrt{\|x\|^2 - 2s\|x\|\sin(\varphi) + s^2}\Big) \\ &\qquad \times \widetilde{g}(s) s^{d-1} \cos^{d-2}(\varphi)\,d\varphi\,ds. \end{aligned}$$

And finally, by the change of variable, $\theta = \varphi + \pi/2$, we get the desired result. □

ETNA
Kent State University and
Johann Radon Institute (RICAM)

Now we will transform the model (2.1) into radial coordinates. Due to the fact that the solution is compactly supported (see Theorem 3.2), we have

$$\begin{aligned}
&\nabla\cdot(V[\vec{\alpha}_p,\gamma_p,P](t,x)P(t,x))\\
&\quad=\nabla\cdot(\vec{\alpha}_p(\gamma_p*(\mathbb{1}_{\Omega_R}P))(t,x)P(t,x))\\
&\quad=\nabla\cdot(\vec{\alpha}_p(\gamma_p*P)(t,x)P(t,x))\\
&\quad=\nabla\cdot(\vec{\alpha}_p(t,x)(\gamma_p*P)(t,x))P(t,x)+(\vec{\alpha}_p(t,x)(\gamma_p*P)(t,x))\cdot\nabla P(t,x)\\
&\quad=\big[\nabla\cdot(\vec{\alpha}_p(t,x))(\gamma_p*P)(t,x)+\vec{\alpha}_p(t,x)\cdot\nabla((\gamma_p*P)(t,x))\big]P(t,x)\\
&\qquad+(\vec{\alpha}_p(t,x)(\gamma_p*P)(t,x))\cdot\nabla P(t,x).
\end{aligned}$$

The directional vector of the velocity $\vec{\alpha}_p$ is assumed to be a radial vector, so it can be written as

$$\vec{\alpha}_p(t,x)=\widetilde{\alpha_p}(t,r)\vec{e}_r,$$

with $\vec{e}_r=x/\|x\|$. So we have

$$\nabla\cdot(\vec{\alpha}_p(t,x))=\frac{d-1}{r}\widetilde{\alpha_p}(t,r)+\frac{\partial\widetilde{\alpha_p}(t,r)}{\partial r}=\frac{1}{r^{d-1}}\frac{\partial}{\partial r}(r^{d-1}\widetilde{\alpha_p}(t,r)),$$

and because

$$\nabla((\gamma_p*P)(t,x))=\frac{\partial\widetilde{(\gamma_p*P)}}{\partial r}(t,r)\vec{e}_r\qquad\text{and}\qquad\nabla P(t,x)=\frac{\partial\widetilde{P}}{\partial r}(t,r)\vec{e}_r,$$

we get the following:

$$\vec{\alpha}_p(t,x)\cdot\nabla((\gamma_p*P)(t,x))=\widetilde{\alpha_p}(t,r)\frac{\partial\widetilde{(\gamma_p*P)}}{\partial r}(t,r)=\widetilde{\alpha_p}(t,r)\frac{\partial\widetilde{\gamma_p}}{\partial r}\mathbin{\widetilde{*}}\widetilde{P}(t,r)$$

and

$$\vec{\alpha}_p(t,x)(\gamma_p*P)(t,x)\cdot\nabla P(t,x)=\widetilde{\alpha_p}(t,r)\widetilde{(\gamma_p*P)}(t,r)\frac{\partial\widetilde{P}}{\partial r}(t,r).$$

Thus, we have

$$\begin{aligned}
&\nabla\cdot(V[\vec{\alpha}_p,\gamma_p,P](t,x)P(t,x))\\
&\quad=\left[\frac{1}{r^{d-1}}\frac{\partial}{\partial r}\big(r^{d-1}\widetilde{\alpha_p}(t,r)\big)(\widetilde{\gamma_p}\mathbin{\widetilde{*}}\widetilde{P})(t,r)+\widetilde{\alpha_p}(t,r)\left(\frac{\partial\widetilde{\gamma_p}}{\partial r}\mathbin{\widetilde{*}}\widetilde{P}\right)(t,r)\right]\widetilde{P}(t,r)\\
&\qquad+\widetilde{\alpha_p}(t,r)(\widetilde{\gamma_p}\mathbin{\widetilde{*}}\widetilde{P})(t,r)\frac{\partial\widetilde{P}}{\partial r}(t,r)\\
&\quad=\widetilde{\alpha_p}(t,r)\frac{\partial((\widetilde{\gamma_p}\mathbin{\widetilde{*}}\widetilde{P})\widetilde{P})}{\partial r}(t,r)+\frac{1}{r^{d-1}}\frac{\partial}{\partial r}\big(r^{d-1}\widetilde{\alpha_p}(t,r)\big)(\widetilde{\gamma_p}\mathbin{\widetilde{*}}\widetilde{P})(t,r)\widetilde{P}(t,r).
\end{aligned}$$

Finally, we can write the equation for the proliferation cells in the system (2.1) in the following form:

$$\begin{aligned}
&\frac{\partial\widetilde{P}}{\partial t}(t,r)+\widetilde{\alpha_p}(t,r)\frac{\partial((\widetilde{\gamma_p}\mathbin{\widetilde{*}}\widetilde{P})\widetilde{P})}{\partial r}(t,r)\\
&\quad=\left(\widetilde{m}(r)H(\widetilde{M}(t,r))-a_1\widetilde{m}(r)\lambda(t)\widetilde{M}(t,r)\right.\\
&\qquad\left.-\frac{1}{r^{d-1}}\frac{\partial}{\partial r}\big(r^{d-1}\widetilde{\alpha_p}(t,r)\big)(\widetilde{\gamma_p}\mathbin{\widetilde{*}}\widetilde{P})(t,r)\right)\widetilde{P}(t,r).
\end{aligned}$$

ETNA
Kent State University and
Johann Radon Institute (RICAM)

In the same way, for the equation of healthy cells, we have

$$\begin{aligned}&\frac{\partial \widetilde{S}}{\partial t}(t,r)+\widetilde{\alpha_s}(t,r)\frac{\partial((\widetilde{\gamma_s}\,\widetilde{*}\,\widetilde{S})\widetilde{S})}{\partial r}(t,r)\\&\quad=\left(-a_2\widetilde{m}(r)\lambda(t)\widetilde{M}(t,r)-\frac{1}{r^{d-1}}\frac{\partial}{\partial r}\big(r^{d-1}\widetilde{\alpha_s}(t,r)\big)(\widetilde{\gamma_s}\,\widetilde{*}\,\widetilde{S})(t,r)\right)\widetilde{S}(t,r).\end{aligned}$$

We recall that

$$\Delta M(t,x)=\Delta\widetilde{M}(t,\|x\|_2)=\frac{d-1}{r}\frac{\partial\widetilde{M}}{\partial r}(t,r)+\frac{\partial^2\widetilde{M}}{\partial r^2}(t,r)=\frac{1}{r^{d-1}}\frac{\partial}{\partial r}\left(r^{d-1}\frac{\partial\widetilde{M}}{\partial r}(t,r)\right).$$

Finally, we write the system (2.1) in radial coordinates as follows:

$$\text{(4.1)}\qquad\begin{cases}\dfrac{\partial\widetilde{P}}{\partial t}(t,r)+\widetilde{\alpha_p}(t,r)\dfrac{\partial}{\partial r}((\widetilde{\gamma_p}\,\widetilde{*}\,\widetilde{P})\widetilde{P})=f_P(t,r)\widetilde{P}(t,r),\\[2ex]\dfrac{\partial\widetilde{S}}{\partial t}(t,r)+\widetilde{\alpha_s}(t,r)\dfrac{\partial}{\partial r}((\widetilde{\gamma_s}\,\widetilde{*}\,\widetilde{S})\widetilde{S})=f_S(t,r)\widetilde{S}(t,r),\\[2ex]\dfrac{\partial\widetilde{M}}{\partial t}(t,r)-\dfrac{D}{r^{d-1}}\dfrac{\partial}{\partial r}\left(r^{d-1}\dfrac{\partial\widetilde{M}}{\partial r}\right)=M_s\widetilde{S}(1-\widetilde{M})-\eta\widetilde{M}\widetilde{P},\\[2ex]\qquad P(t,R)=0,\quad S(t,R)=S_R,\quad M(t,R)=M_R,\\\qquad P(0,r)=P_0(r),\quad S(0,r)=S_0(r),\quad M(0,r)=M_0(r),\end{cases}$$

where $(t,r)\in[0,T]\times]0,R]$ and

$$\begin{aligned}f_P(t,r)&=\widetilde{m}(r)H(\widetilde{M}(t,r))-a_1\widetilde{m}(r)\lambda(t)\widetilde{M}(t,r)\\&\quad-\frac{1}{r^{d-1}}\frac{\partial}{\partial r}(r^{d-1}\widetilde{\alpha_p}(t,r))(\widetilde{\gamma_p}\,\widetilde{*}\,\widetilde{P})(t,r),\\f_S(t,r)&=-a_2\widetilde{m}(r)\lambda(t)\widetilde{M}(t,r)-\frac{1}{r^{d-1}}\frac{\partial}{\partial r}(r^{d-1}\widetilde{\alpha_s}(t,r))(\widetilde{\gamma_s}\,\widetilde{*}\,\widetilde{S})(t,r).\end{aligned}$$

We denote by $\widetilde{U}=(\widetilde{P},\widetilde{S},\widetilde{M})$ the exact solution of the radial problem (4.1). Then the system (4.1) may be written as

$$\text{(4.2)}\qquad\begin{cases}\dfrac{\partial\widetilde{U}}{\partial t}(t,r)+\widetilde{\mathcal{A}}(\widetilde{U})(t,r)=\widetilde{G}(\widetilde{U})(t,r), & (t,r)\in[0,T]\times]0,R],\\[2ex]\widetilde{U}(t,R)=\widetilde{U}_R, & t\in[0,T],\\\widetilde{U}(0,r)=\widetilde{U}_0(r), & r\in]0,R],\end{cases}$$

with

$$\begin{aligned}\widetilde{\mathcal{A}}(\widetilde{U})(t,r)&=\left[\widetilde{\alpha_p}(t,r)\frac{\partial}{\partial r}((\widetilde{\gamma_p}\,\widetilde{*}\,\widetilde{P})\widetilde{P}),\ \widetilde{\alpha_s}(t,r)\frac{\partial}{\partial r}((\widetilde{\gamma_s}\,\widetilde{*}\,\widetilde{S})\widetilde{S}),\ -\frac{D}{r^{d-1}}\frac{\partial}{\partial r}\left(r^{d-1}\frac{\partial\widetilde{M}}{\partial r}\right)\right],\\\widetilde{G}(\widetilde{U})(t,r)&=\Big(\widetilde{g}_1(\widetilde{U})(t,r),\ \widetilde{g}_2(\widetilde{U})(t,r),\ \widetilde{g}_3(\widetilde{U})(t,r)\Big),\end{aligned}$$

ETNA
Kent State University and
Johann Radon Institute (RICAM)

where

$$\widetilde{g}_1(\widetilde{U})(t,r) = \Bigg(\widetilde{m}(r)H(\widetilde{M}(t,r)) - a_1\widetilde{m}(r)\lambda(t)\widetilde{M}(t,r) - \frac{1}{r^{d-1}}\frac{\partial}{\partial r}(r^{d-1}\widetilde{\alpha_p}(t,r))(\widetilde{\gamma_p} \,\widetilde{*}\, \widetilde{P})(t,r)\Bigg)\widetilde{P}(t,r),$$

$$\widetilde{g}_2(\widetilde{U})(t,r) = \Bigg(-a_2\widetilde{m}(r)\lambda(t)\widetilde{M}(t,r) - \frac{1}{r^{d-1}}\frac{\partial}{\partial r}(r^{d-1}\widetilde{\alpha_s}(t,r))(\widetilde{\gamma_s} \,\widetilde{*}\, \widetilde{S})(t,r)\Bigg)\widetilde{S}(t,r),$$

$$\widetilde{g}_3(\widetilde{U})(t,r) = M_s\widetilde{S}(t,r)(1-\widetilde{M}(t,r)) - \eta\widetilde{M}(t,r)\widetilde{P}(t,r),$$

$$U_R = (0, S_R, M_R), \qquad \text{and} \qquad U_0 = (P_0, S_0, M_0).$$

5. The collocation method. In this section we describe the collocation method used to solve the radial system (4.2). The method is based on cubic B-splines, which are widely used in numerical analysis because of their smoothness and local approximation properties [8, 12]. B-splines are piecewise polynomial functions that ensure continuity up to the second derivative, making them well-suited for interpolation and for the numerical solution of differential equations, including various classes of partial integro-differential equations [8, 17, 19].

We first subdivide the computational interval into N equal subintervals with nodes

$$r_i = i\,h, \quad \text{for } i = 0, 1, \ldots, N \text{ and } h = R/N,$$

so that the grid points on $[0, R]$ are given by $r_0 = 0, r_1, \ldots, r_N = R$. For the B-spline construction we then use an extended uniform partition obtained by adjoining three extra knots at each end. Explicitly, we keep the subdivision block

$$r_{-3} < r_{-2} < r_{-1} < 0 = r_0 < r_1 < \cdots < r_N = R < r_{N+1} < r_{N+2} < r_{N+3}.$$

Adding three knots per side is standard for cubic splines. It ensures that all boundary basis functions are fully defined while preserving the compact support $\operatorname{supp} B_i = [r_{i-2}, r_{i+2}]$ and the approximation order. The resulting basis $\{B_i(r)\}_{i=-1}^{N+1}$ spans an $(N+3)$-dimensional space on $[0, R]$.

In this context, the fundamental B-spline function refers to the cubic spline centered at the nodes $-2, -1, 0, 1, 2$, and its support is limited to the interval $[-2, 2]$. It can be written as follows:

$$B(r) = \begin{cases} 0 & \text{if } r < -2 \text{ or } r \geq 2, \\ \frac{1}{6}(2+r)^3 & \text{if } -2 \leq r < -1, \\ \frac{1}{6}(4 - 6r^2 - 3r^3) & \text{if } -1 \leq r < 0, \\ \frac{1}{6}(4 - 6r^2 + 3r^3) & \text{if } 0 \leq r < 1, \\ \frac{1}{6}(2-r)^3 & \text{if } 1 \leq r < 2, \end{cases}$$

and B_i represent the well-known B-spline functions associated to the nodes r_i defined for $i = -1, \ldots, N+1$ by

$$B_i(r) = B\left(\frac{r - r_i}{h}\right).$$

The function B_i is compactly supported on the interval $[r_{i-2}, r_{i+2}]$. Table 5.1 provides a summary of the values of B_i and its derivatives at the points r_i.

ETNA
Kent State University and
Johann Radon Institute (RICAM)

TABLE 5.1
Values of B-splines and their derivatives at the points r_i.

x	r_{i-2}	r_{i-1}	r_i	r_{i+1}	r_{i+2}
$B_i(r)$	0	$1/6$	$4/6$	$1/6$	0
$B_i'(r)$	0	$-1/2h$	0	$1/2h$	0
$B_i''(r)$	0	$1/h^2$	$-2/h^2$	$1/h^2$	0

The exact solution of (4.2) is approximated by a cubic B-spline given by the following expression:

$$\begin{aligned}\widetilde{U}_h(t,r) &= \left(\widetilde{P}_h(t,r), \widetilde{S}_h(t,r), \widetilde{M}_h(t,r)\right) \\ &= \left(\sum_{i=-1}^{N+1} \alpha_i^{(1)}(t)B_i(r), \sum_{i=-1}^{N+1} \alpha_i^{(2)}(t)B_i(r), \sum_{i=-1}^{N+1} \alpha_i^{(3)}(t)B_i(r)\right),\end{aligned}$$

where $\alpha_i^{(k)}(t)$ are time-dependent coefficients with unknown values for $k = 1, 2, 3$.

Let us consider the following vector-valued functions of dimensions $(N-1)\times 1$ and $3(N-1)\times 1$, respectively:

$$\mathbb{B}(r) = \left(B_1(r), B_2(r), \ldots, B_{N-1}(r)\right)^T \quad \text{and} \quad \alpha(t) = \left(\alpha^{(1)}(t)^T, \alpha^{(2)}(t)^T, \alpha^{(3)}(t)^T\right)^T,$$

with

$$\alpha^{(k)}(t) = \left(\alpha_1^{(k)}(t), \alpha_2^{(k)}(t), \ldots, \alpha_{N-1}^{(k)}(t)\right)^T, \quad k = 1, 2, 3.$$

The function $U_h(t,x)$ has the form

$$\widetilde{U_h}(t,r) = \begin{bmatrix} \alpha_{-1}^{(1)}(t)B_{-1}(r) + \alpha_0^{(1)}(t)B_0(r) + \mathbb{B}(r)^T\alpha^{(1)}(t) \\ \quad + \alpha_N^{(1)}(t)B_N(r) + \alpha_{N+1}^{(1)}(t)B_{N+1}(r) \\ \alpha_{-1}^{(2)}(t)B_{-1}(r) + \alpha_0^{(2)}(t)B_0(r) + \mathbb{B}(r)^T\alpha^{(2)}(t) \\ \quad + \alpha_N(t)^{(2)}B_N(r) + \alpha_{N+1}^{(2)}(t)B_{N+1}(r) \\ \alpha_{-1}^{(3)}(t)B_{-1}(r) + \alpha_0^{(3)}(t)B_0(r) + \mathbb{B}(r)^T\alpha^{(3)}(t) \\ \quad + \alpha_N(t)^{(3)}B_N(r) + \alpha_{N+1}^{(3)}(t)B_{N+1}(r) \end{bmatrix}, \tag{5.1}$$

where the notation $\mathbb{B}(r)^T$ is used for the transpose of the vector $\mathbb{B}(r)$.

The collocation method involves substituting $\widetilde{U_h}$ and its derivatives in (4.2) with the expression for $\widetilde{U_h}$ given by (5.1). This substitution is followed by evaluating the resulting equation at the points r_i, for $i = 0, \ldots, N$. Consequently, we obtain an ODE that we can solve later. Beginning with the first equation for tumor cells $\widetilde{P_h}$, we have

$$\frac{\partial \widetilde{P}_h}{\partial t}(t,r) + \widetilde{\alpha_p}(t,r)\frac{\partial((\widetilde{\gamma_p} \mathbin{\widetilde{*}} \widetilde{P}_h)\widetilde{P}_h)}{\partial r}(t,r) = \widetilde{g}_1(\widetilde{U}_h)(t,r),$$

ETNA
Kent State University and
Johann Radon Institute (RICAM)

which may be written in the form

$$\begin{aligned}\frac{\partial \widetilde{P}_h}{\partial t}(t,r) + (\widetilde{\gamma_p} \mathbin{\widetilde{*}} \widetilde{P}_h)(t,r)\left[\frac{1}{r^{d-1}}\frac{\partial}{\partial r}(r^{d-1}\widetilde{\alpha_p}(t,r))\widetilde{P}_h(t,r) + \widetilde{\alpha_p}(t,r)\frac{\partial \widetilde{P}_h}{\partial r}(t,r)\right] \\ + \left(\frac{\partial \widetilde{\gamma_p}}{\partial r} \mathbin{\widetilde{*}} \widetilde{P}_h\right)(t,r)\widetilde{P}_h(t,r) \\ = \Big(H(\widetilde{M}_h(t,r)) - a_1\lambda(t)\widetilde{M}_h(t,r)\Big)\widetilde{P}_h(t,r).\end{aligned}$$

We start by first expressing the nonlocal term. We have

$$(\widetilde{\gamma_p} \mathbin{\widetilde{*}} \widetilde{P}_h)(t,r) = \left(\widetilde{\gamma_p} \mathbin{\widetilde{*}} \left(\sum_{i=-1}^{N+1} \alpha_i^{(1)}(t)B_i\right)\right)(t,r) = \sum_{i=-1}^{N+1} \alpha_i^{(1)}(t)\left(\widetilde{\gamma_p} \mathbin{\widetilde{*}} B_i\right)(r). \tag{5.2}$$

For $i = -1, \ldots, N+1$ and $k = p, s$, we note that

$$\mathrm{Z}_i^k(r) := (\widetilde{\gamma_k} \mathbin{\widetilde{*}} B_i)(r) \quad \text{and} \quad \overline{\mathrm{Z}}_i^k(r) := \frac{\partial(\widetilde{\gamma_k} \mathbin{\widetilde{*}} B_i)(r)}{\partial r} = \left(\frac{\partial \widetilde{\gamma_k}}{\partial r} \mathbin{\widetilde{*}} B_i\right)(r).$$

Then by substituting in (5.2), we get

$$\begin{aligned}&\sum_{i=-1}^{N+1} \frac{d\alpha_i^{(1)}}{dt}(t)B_i(r) + \sum_{i=-1}^{N+1} \alpha_i^{(1)}(t)\mathrm{Z}_i^p(r) \\ &\quad\times\left[\frac{1}{r^{d-1}}\frac{\partial}{\partial r}\big(r^{d-1}\widetilde{\alpha_p}(t,r)\big)\sum_{i=-1}^{N+1}\alpha_i^{(1)}(t)B_i(r) + \widetilde{\alpha_p}(t,r)\sum_{i=-1}^{N+1}\alpha_i^{(1)}(t)B_i'(r)\right] \\ &\quad+\widetilde{\alpha_p}(t,r)\sum_{i=-1}^{N+1}\alpha_i^{(1)}(t)\overline{\mathrm{Z}}_i^p(r)\sum_{i=-1}^{N+1}\alpha_i^{(1)}(t)B_i(r) \\ &= \left(H\left(\sum_{i=-1}^{N+1}\alpha_i^{(3)}(t)B_i(r)\right) - a_1\lambda(t)\sum_{i=-1}^{N+1}\alpha_i^{(3)}(t)B_i(r)\right)\sum_{i=-1}^{N+1}\alpha_i^{(1)}(t)B_i(r).\end{aligned} \tag{5.3}$$

For the healthy cells $\widetilde{S_h}$, similar calculations lead to

$$\begin{aligned}&\sum_{i=-1}^{N+1} \frac{d\alpha_i^{(2)}}{dt}(t)B_i(r) + \sum_{i=-1}^{N+1} \alpha_i^{(2)}(t)\mathrm{Z}_i^s(r) \\ &\quad\times\left[\frac{1}{r^{d-1}}\frac{\partial}{\partial r}\big(r^{d-1}\widetilde{\alpha_s}(t,r)\big)\sum_{i=-1}^{N+1}\alpha_i^{(2)}(t)B_i(r) + \widetilde{\alpha_s}(t,r)\sum_{i=-1}^{N+1}\alpha_i^{(2)}(t)B_i'(r)\right] \\ &\quad+\widetilde{\alpha_s}(t,r)\sum_{i=-1}^{N+1}\alpha_i^{(2)}(t)\overline{\mathrm{Z}}_i^s(r)\sum_{i=-1}^{N+1}\alpha_i^{(2)}(t)B_i(r) \\ &= -a_2\lambda(t)\sum_{i=-1}^{N+1}\alpha_i^{(3)}(t)B_i(r)\sum_{i=-1}^{N+1}\alpha_i^{(2)}(t)B_i(r).\end{aligned}$$

ETNA
Kent State University and
Johann Radon Institute (RICAM)

Similarly, for the third equation describing the concentration of oxygen and nutrients in the tissue, we have

$$\begin{aligned}\sum_{i=-1}^{N+1}\frac{d\alpha_i^{(3)}}{dt}(t)B_i(r) - D\left(\frac{d-1}{r}\sum_{i=-1}^{N+1}\alpha_i^{(3)}(t)B_i'(r) + \sum_{i=-1}^{N+1}\alpha_i^{(3)}(t)B_i''(r)\right)\\ = M_s\sum_{i=-1}^{N+1}\alpha_i^{(2)}(t)B_i(r)\left(1-\sum_{i=-1}^{N+1}\alpha_i^{(3)}(t)B_i(r)\right)\\ -\eta\sum_{i=-1}^{N+1}\alpha_i^{(3)}(t)B_i(r)\sum_{i=-1}^{N+1}\alpha_i^{(1)}(t)B_i(r).\end{aligned}$$

To determine the values of α at the boundaries, we consider $\widetilde{U}_h = (\widetilde{P}_h, \widetilde{S}_h, \widetilde{M}_h)^T$ as natural cubic splines. Natural cubic splines require that their second derivatives vanish at the endpoints of the interval $[0, R]$. Hence, we have

$$\frac{\partial^2\widetilde{U_h}}{\partial r^2}(t, r_0) = \frac{1}{h^2}\Big(\alpha_{-1}^{(j)}(t) - 2\alpha_0^{(j)}(t) + \alpha_1^{(j)}(t)\Big)_{j=1,2,3}^T = \mathbf{0},$$

which leads to

$$\alpha_{-1}^j(t) = 2\alpha_0^j(t) - \alpha_1^j(t), \qquad \text{for } j = 1, 2, 3. \tag{5.4}$$

On the other hand, we set the value of the solution at the point $r = r_0$ to be fixed and denote it by $U_h(t, r_0) := (P_L(t), S_L(t), M_L(t))^T$. Then we have

$$\begin{aligned}\widetilde{U_h}(t, r_0) &= \tfrac{1}{6}\left(\alpha_{-1}^{(j)}(t) + 4\alpha_0^{(j)}(t) + \alpha_1^{(j)}(t)\right)_{j=1,2,3}^T\\ &= \left(\alpha_0^{(j)}(t)\right)_{j=1,2,3}^T = (P_L(t), S_L(t), M_L(t))^T.\end{aligned} \tag{5.5}$$

By analogous observations, we get for $r = r_{N+1} = R$ the following:

$$\alpha_{N+1}^j(t) = 2\alpha_N^j(t) - \alpha_{N-1}^j(t), \qquad \text{for } j = 1, 2, 3 \tag{5.6}$$

and

$$\left(\alpha_{N+1}^{(1)}(t), \alpha_{N+1}^{(2)}(t), \alpha_{N+1}^{(3)}(t)\right)^T = (P_R, S_R, M_R)^T. \tag{5.7}$$

Now, let us note for $k = p, s$ the following vector-valued functions of size $N-1$:

$$\mathbb{Z}_k(r) := \left(\mathrm{Z}_1^k(r) - \mathrm{Z}_{-1}^k(r), \mathrm{Z}_2^k(r), \ldots, \mathrm{Z}_{N-2}^k(r), \mathrm{Z}_{N-1}^k(r) - \mathrm{Z}_{N+1}^k(r)\right)^T, \tag{5.8}$$

and

$$\overline{\mathbb{Z}}_k(r) := \left(\overline{\mathrm{Z}}_1^k(r) - \overline{\mathrm{Z}}_{-1}^k(r), \overline{\mathrm{Z}}_2^k(r), \ldots, \overline{\mathrm{Z}}_{N-2}^k(r), \overline{\mathrm{Z}}_{N-1}^k(r) - \overline{\mathrm{Z}}_{N+1}^k(r)\right)^T. \tag{5.9}$$

Furthermore, we define the functions

$$\begin{aligned}\mathrm{Q}_p(r) &:= P_L(t)\big(2\mathrm{Z}_{-1}^p(r) + \mathrm{Z}_0^p(r)\big) + P_R\big(2\mathrm{Z}_{N+1}^p(r) + \mathrm{Z}_{N+1}^p(r)\big),\\ \overline{\mathrm{Q}}_p(r) &:= P_L(t)\big(2\overline{\mathrm{Z}}_{-1}^p(r) + \overline{\mathrm{Z}}_0^p(r)\big) + P_R\big(2\overline{\mathrm{Z}}_{N+1}^p(r) + \overline{\mathrm{Z}}_{N+1}^p(r)\big),\\ \mathrm{Q}_s(r) &:= S_L(t)\big(2\mathrm{Z}_{-1}^s(r) + \mathrm{Z}_0^s(r)\big) + S_R\big(2\mathrm{Z}_{N+1}^s(r) + \mathrm{Z}_{N+1}^s(r)\big),\\ \overline{\mathrm{Q}}_s(r) &:= S_L(t)\big(2\overline{\mathrm{Z}}_{-1}^s(r) + \overline{\mathrm{Z}}_0^s(r)\big) + S_R\big(2\overline{\mathrm{Z}}_{N+1}^s(r) + \overline{\mathrm{Z}}_{N+1}^s(r)\big).\end{aligned} \tag{5.10}$$

ETNA
Kent State University and
Johann Radon Institute (RICAM)

Using the natural spline boundary conditions (5.4), (5.5), (5.6), and (5.7), and the notation (5.8), (5.9), and (5.10), the nonlocal terms can be expressed compactly as

$$\sum_{i=-1}^{N+1} \alpha_i^{(1)}(t)\mathrm{Z}_i^p(r) = \mathrm{Q}_p(r) + \mathbb{Z}_p^T(r)\alpha^{(1)}(t), \qquad \sum_{i=-1}^{N+1} \alpha_i^{(1)}(t)\overline{\mathrm{Z}}_i^p(r) = \overline{\mathrm{Q}_p}(r) + \overline{\mathbb{Z}}_p^T(r)\alpha^{(1)}(t),$$
$$\sum_{i=-1}^{N+1} \alpha_i^{(2)}(t)\mathrm{Z}_i^s(r) = \mathrm{Q}_s(r) + \mathbb{Z}_s^T(r)\alpha^{(2)}(t), \qquad \sum_{i=-1}^{N+1} \alpha_i^{(2)}(t)\overline{\mathrm{Z}}_i^s(r) = \overline{\mathrm{Q}_s}(r) + \overline{\mathbb{Z}}_s^T(r)\alpha^{(2)}(t).$$

Now we express $\widetilde{U_h}$ at the points r_i, for $i = 0, \ldots, N$. We start with equation (5.3) at $r = r_0$ and obtain

$$\begin{aligned}
\frac{d\alpha_0^{(1)}}{dt}(t) &= -(\mathrm{Q}_p(r_0) + \mathbb{Z}_p^T(r_0)\alpha^{(1)}(t)) \\
&\quad \times \left[\frac{1}{r_0^{d-1}}\left(\frac{\partial(r^{d-1}\widetilde{\alpha_p})}{\partial r}(t, r_0)\right) P_L(t) + \widetilde{\alpha_p}(t, r_0)\frac{1}{h}(\alpha_1^{(1)}(t) - P_L(t))\right] \\
&\quad - \widetilde{\alpha_p}(t, r_0)\Big(\overline{\mathrm{Q}_p}(r_0) + \overline{\mathbb{Z}}_p^T(r_0)\alpha^{(1)}(t)\Big)P_L(t) \\
&\quad + [H(M_L(t)) - a_1\lambda(t)M_L(t)]P_L(t), \\
\frac{d\alpha_0^{(2)}}{dt}(t) &= -(\mathrm{Q}_s(r_0) + \mathbb{Z}_s^T(r_0)\alpha^{(2)}(t)) \\
&\quad \times \left[\frac{1}{r_0^{d-1}}\left(\frac{\partial(r^{d-1}\widetilde{\alpha_s})}{\partial r}(t, r_0)\right) S_L(t) + \widetilde{\alpha_s}(t, r_0)\frac{1}{h}(\alpha_1^{(1)}(t) - S_L(t))\right] \\
&\quad - \widetilde{\alpha_s}(t, r_0)\Big(\overline{\mathrm{Q}_s}(r_0) + \overline{\mathbb{Z}}_s^T(r_0)\alpha^{(2)}(t)\Big)S_L(t) \\
&\quad - a_2\lambda(t)M_L(t)S_L(t), \\
\frac{d\alpha_0^{(3)}}{dt}(t) &= \frac{D(d-1)}{rh}(\alpha_1^{(3)}(t) - M_L(t)) + M_sS_L(t)(1 - M_L(t)) - \eta M_L(t)P_L(t).
\end{aligned}$$

By substituting at $r = r_i$, for $i = 1, \ldots, N-1$, we get

$$\begin{aligned}
&\frac{1}{6}\left(\frac{d\alpha_{i-1}^{(1)}}{dt}(t) + 4\frac{d\alpha_i^{(1)}}{dt}(t) + \frac{d\alpha_{i+1}^{(1)}}{dt}(t)\right) \\
&\quad = -\big(\mathrm{Q}_p(r_i) + \mathbb{Z}_p^T(r_i)\alpha^{(1)}(t)\big) \\
&\qquad \times \left[\frac{1}{r_i^{d-1}}\left(\frac{\partial(r^{d-1}\widetilde{\alpha_p})}{\partial r}(t, r_i)\right)\frac{1}{6}\big(\alpha_{i-1}^{(1)}(t) + 4\alpha_i^{(1)}(t) + \alpha_{i+1}^{(1)}(t)\big)\right. \\
&\qquad\quad \left. + \widetilde{\alpha_p}(t, r_i)\frac{1}{2h}\big(\alpha_{i+1}^{(1)}(t) - \alpha_{i-1}^{(1)}(t)\big)\right] \\
&\qquad - \frac{1}{6}\widetilde{\alpha_p}(t, r_i)\Big(\overline{\mathrm{Q}_p}(r_i) + \overline{\mathbb{Z}}_p^T(r_i)\alpha^{(1)}(t)\Big)\big(\alpha_{i-1}^{(1)}(t) + 4\alpha_i^{(1)}(t) + \alpha_{i+1}^{(1)}(t)\big) \\
&\qquad + \left[H\left(\frac{1}{6}\big(\alpha_{i-1}^{(3)}(t) + 4\alpha_i^{(3)}(t) + \alpha_{i+1}^{(3)}(t)\big)\right)\right.
\end{aligned}$$

ETNA
Kent State University and
Johann Radon Institute (RICAM)

$$
\begin{aligned}
&\quad - \frac{1}{6}a_1\lambda(t)\big(\alpha_{i-1}^{(3)}(t) + 4\alpha_i^{(3)}(t) + \alpha_{i+1}^{(3)}(t)\big)\Bigg] \\
&\quad \times \frac{1}{6}\big(\alpha_{i-1}^{(1)}(t) + 4\alpha_i^{(1)}(t) + \alpha_{i+1}^{(1)}(t)\big), \\
&\frac{1}{6}\left(\frac{d\alpha_{i-1}^{(2)}}{dt}(t) + 4\frac{d\alpha_i^{(2)}}{dt}(t) + \frac{d\alpha_{i+1}^{(2)}}{dt}(t)\right) \\
&\quad = -\big(\mathrm{Q}_s(r_i) + \mathbb{Z}_s^T(r_i)\alpha^{(2)}(t)\big) \\
&\qquad \times \left[\frac{1}{r_i^{d-1}}\left(\frac{\partial(r^{d-1}\widetilde{\alpha_s})}{\partial r}(t, r_i)\right)\frac{1}{6}\big(\alpha_{i-1}^{(2)}(t) + 4\alpha_i^{(2)}(t) + \alpha_{i+1}^{(2)}(t)\big)\right. \\
&\qquad\quad \left. + \widetilde{\alpha_s}(t, r_i)\frac{1}{2h}\big(\alpha_{i+1}^{(2)}(t) - \alpha_{i-1}^{(2)}(t)\big)\right] \\
&\qquad - \frac{1}{6}\widetilde{\alpha_s}(t, r_i)\Big(\overline{\mathrm{Q}_s}(r_i) + \overline{\mathbb{Z}}_s^T(r_i)\alpha^{(2)}(t)\Big)\big(\alpha_{i-1}^{(2)}(t) + 4\alpha_i^{(2)}(t) + \alpha_{i+1}^{(2)}(t)\big) \\
&\qquad - \frac{1}{36}a_2\lambda(t)\big(\alpha_{i-1}^{(3)}(t) + 4\alpha_i^{(3)}(t) + \alpha_{i+1}^{(3)}(t)\big)\big(\alpha_{i-1}^{(2)}(t) + 4\alpha_i^{(2)}(t) + \alpha_{i+1}^{(2)}(t)\big),
\end{aligned}
$$

and

$$
\begin{aligned}
&\frac{1}{6}\left(\frac{d\alpha_{i-1}^{(3)}}{dt}(t) + 4\frac{d\alpha_i^{(3)}}{dt}(t) + \frac{d\alpha_{i+1}^{(3)}}{dt}(t)\right) \\
&\quad = D\left(\frac{d-1}{2rh}\big(\alpha_{i+1}^{(3)}(t) - \alpha_{i-1}^{(3)}(t)\big) + \frac{1}{h^2}\big(\alpha_{i-1}^{(3)}(t) - 2\alpha_i^{(3)}(t) + \alpha_{i+1}^{(3)}(t)\big)\right) \\
&\qquad + \frac{M_s}{6}\big(\alpha_{i-1}^{(2)}(t) + 4\alpha_i^{(2)}(t) + \alpha_{i+1}^{(2)}(t)\big)\left(1 - \frac{1}{6}\big(\alpha_{i-1}^{(3)}(t) + 4\alpha_i^{(3)}(t) + \alpha_{i+1}^{(3)}(t)\big)\right) \\
&\qquad - \eta\frac{1}{36}\big(\alpha_{i-1}^{(3)}(t) + 4\alpha_i^{(3)}(t) + \alpha_{i+1}^{(3)}(t)\big)\big(\alpha_{i-1}^{(1)}(t) + 4\alpha_i^{(1)}(t) + \alpha_{i+1}^{(1)}(t)\big).
\end{aligned}
$$

Finally we get for $r = r_N = R$ the following:

$$
\begin{aligned}
\frac{d\alpha_N^{(1)}}{dt}(t) &= -\big(\mathrm{Q}_p(r_N) + \mathbb{Z}_p^T(r_N)\alpha^{(1)}(t)\big) \\
&\qquad \times \left[\frac{1}{r_N^{d-1}}\left(\frac{\partial(r^{d-1}\widetilde{\alpha_p})}{\partial r}(t, r_N)\right)P_R + \widetilde{\alpha_p}(t, r_N)\frac{1}{h}\big(P_R - \alpha_{N-1}^{(1)}(t)\big)\right] \\
&\qquad - \widetilde{\alpha_p}(t, r_N)\Big(\overline{\mathrm{Q}_p}(r_N) + \overline{\mathbb{Z}}_p^T(r_N)\alpha^{(1)}(t)\Big)P_R \\
&\qquad + [H(M_R) - a_1\lambda(t)M_R]P_R, \\
\frac{d\alpha_N^{(2)}}{dt}(t) &= -\big(\mathrm{Q}_s(r_N) + \mathbb{Z}_s^T(r_N)\alpha^{(2)}(t)\big) \\
&\qquad \times \left[\frac{1}{r_N^{d-1}}\left(\frac{\partial(r^{d-1}\widetilde{\alpha_s})}{\partial r}(t, r_N)\right)S_R + \widetilde{\alpha_s}(t, r_N)\frac{1}{h}\big(S_R - \alpha_{N-1}^{(2)}(t)\big)\right] \\
&\qquad - \widetilde{\alpha_s}(t, r_N)\left(\overline{\mathrm{Q}_s}(r_N) + \overline{\mathbb{Z}}_s^T(r_N)\alpha^{(2)}(t)\right)S_R \\
&\qquad - a_2\lambda(t)M_RS_R, \\
\frac{d\alpha_N^{(3)}}{dt}(t) &= \frac{D(d-1)}{rh}\big(M_R - \alpha_{N-1}^{(3)}(t)\big) + M_sS_R(t)(1 - M_R) - \eta M_RP_R.
\end{aligned}
$$

ETNA
Kent State University and
Johann Radon Institute (RICAM)

For the initial time $t = 0$, the B-spline interpolation conditions yield the linear system

$$\mathbb{A}\boldsymbol{\alpha}(0) = \widetilde{\mathbf{U}}^0,$$

where $\mathbb{A} = \text{diag}(A, A, A)$ is a $3(N-1) \times 3(N-1)$ block diagonal matrix, with A being the $(N-1) \times (N-1)$ tridiagonal matrix

$$A = \tfrac{1}{6}(\text{diag}(\mathbf{1}_{N-2}, -1) + \text{diag}(\mathbf{4}_{N-1}, 0) + \text{diag}(\mathbf{1}_{N-2}, 1)).$$

Here $\mathbf{1}_n$ and $\mathbf{4}_n$ denote vectors of 1s and 4s of length n, respectively, and the notation $\text{diag}(\mathbf{v}, k)$ represents a matrix with vector $\mathbf{v}$ on the kth diagonal. The right-hand side vector $\widetilde{\mathbf{U}}^0 = (\widetilde{\mathbf{U}}^{0,(1)}, \widetilde{\mathbf{U}}^{0,(2)}, \widetilde{\mathbf{U}}^{0,(3)})^T$ contains the initial data with each block defined as

$$\widetilde{\mathbf{U}}^{0,(k)} = \left(\widetilde{U}_k^0(r_1) - \tfrac{1}{6}\widetilde{U}_k^0(r_0),\ \widetilde{U}_k^0(r_2), \ldots, \widetilde{U}_k^0(r_{N-2}),\ \widetilde{U}_k^0(r_{N-1}) - \tfrac{1}{6}\widetilde{U}_k^0(r_N)\right)^T,$$

where $\widetilde{U}_1^0 = \widetilde{P}_0$, $\widetilde{U}_2^0 = \widetilde{S}_0$, and $\widetilde{U}_3^0 = \widetilde{M}_0$.

Subsequently, $\boldsymbol{\alpha}$ satisfies the following ODE:

$$\begin{cases} \mathbb{A}\dfrac{d\boldsymbol{\alpha}}{dt}(t) = \boldsymbol{\Phi}(t, \boldsymbol{\alpha}(t)), \quad t \in [0, T], \\ \mathbb{A}\boldsymbol{\alpha}(0) = \widetilde{\mathbf{U}}^0, \end{cases} \tag{5.11}$$

where the nonlinear function $\boldsymbol{\Phi}(t, \boldsymbol{\alpha}(t))$ can be expressed as

$$\begin{aligned} \boldsymbol{\Phi}(t, \boldsymbol{\alpha}(t)) = &-\text{diag}(\mathbb{M}_Z^p, \mathbb{M}_Z^s, \mathbf{0})\boldsymbol{\alpha}(t) - (\mathbb{M}_Q^p, \mathbb{M}_Q^s, \mathbf{0})^T \\ &\odot [(\overline{\mathbb{M}}_{\tilde{\alpha}}^p(t), \overline{\mathbb{M}}_{\tilde{\alpha}}^s(t), \mathbf{0})^T \odot \mathbb{A} + (\mathbb{M}_{\tilde{\alpha}}^p, \mathbb{M}_{\tilde{\alpha}}^s, \mathbf{0})^T \odot \text{diag}(A', A', \mathbf{0})]\boldsymbol{\alpha}(t) \\ &+ \boldsymbol{G}(t, \boldsymbol{\alpha}(t)) + \boldsymbol{f}(t, \boldsymbol{\alpha}(t)). \end{aligned}$$

Here the matrices A' and A'' are defined using the diag-notation as

$$\begin{aligned} A' &= \frac{-1}{2h}(\text{diag}(\mathbf{1}_{N-2}, -1) + \text{diag}(\mathbf{1}_{N-2}, 1)), \\ A'' &= \frac{1}{h^2}(\text{diag}(\mathbf{1}_{N-2}, -1) - 2\,\text{diag}(\mathbf{1}_{N-1}, 0) + \text{diag}(\mathbf{1}_{N-2}, 1)), \end{aligned}$$

and

$$\begin{aligned} \mathbb{M}_Z^k &= (\mathbb{Z}_k(r_1), \ldots, \mathbb{Z}_k(r_{N-1}))^T, \quad \overline{\mathbb{M}}_Z^k = (\overline{\mathbb{Z}}_k(r_1), \ldots, \overline{\mathbb{Z}}_k(r_{N-1}))^T, \quad k = p, s, \\ \mathbb{M}_Q^k &= (Q_k(r_1), \ldots, Q_k(r_{N-1}))^T, \quad \overline{\mathbb{M}}_Q^k = (\overline{Q}_k(r_1), \ldots, \overline{Q}_k(r_{N-1}))^T, \\ \mathbb{M}_{\tilde{\alpha}}^k(t) &= (\widetilde{\alpha_k}(t, r_1), \ldots, \widetilde{\alpha_k}(t, r_{N-1}))^T, \\ \overline{\mathbb{M}}_{\tilde{\alpha}}^k(t) &= \left(\frac{1}{r_1^{d-1}}\frac{\partial}{\partial r}(r^{d-1}\widetilde{\alpha_k}(t, r_1)), \ldots, \frac{1}{r_{N-1}^{d-1}}\frac{\partial}{\partial r}(r^{d-1}\widetilde{\alpha_k}(t, r_{N-1}))\right)^T, \\ V_M(t) &= \left(\frac{M_L(t)}{6}, 0, \ldots, 0, \frac{M_R}{6}\right)^T, \\ \overline{r}_d &= (d-1)\left(\frac{1}{r_1^{d-1}}, \ldots, \frac{1}{r_{N-1}^{d-1}}\right)^T, \quad \mathbb{1} = (1, \ldots, 1)^T. \end{aligned}$$

ETNA
Kent State University and
Johann Radon Institute (RICAM)

Above, the notation $\odot$ stands for the Hadamard product. Furthermore, the growth and reaction terms are given by

$$\boldsymbol{G}(t,\boldsymbol{\alpha}(t)) = \begin{bmatrix} \{H(A\alpha^{(3)}(t)+V_M(t)) - a_1\lambda(t)A\alpha^{(3)}(t)\} \odot (A\alpha^{(1)}(t)) \\ -\, a_2\lambda(t)(A\alpha^{(3)}(t)) \odot (A\alpha^{(2)}(t)) \\ D(\overline{r}_d \odot A' + A'')\alpha^{(3)}(t) \\ +\, M_s(A\alpha^{(2)}(t)) \odot (\mathbb{1} - A\alpha^{(3)}(t)) - \eta(A\alpha^{(3)}(t)) \odot (A\alpha^{(1)}(t)) \end{bmatrix},$$

while the boundary correction vector $\boldsymbol{f}(t,\boldsymbol{\alpha}(t))$ is a $3(N-1)\times 1$ vector with the following nonzero components:

$$\begin{aligned} f_1(t,\boldsymbol{\alpha}(t)) = &-\frac{1}{6}\frac{d\alpha_0^{(1)}}{dt}(t) - \big(Q_p(r_1) + \mathbb{Z}_p^T(r_1)\alpha^{(1)}(t)\big) \\ &\quad\times\left[\frac{1}{6r_1^{d-1}}\frac{\partial(r^{d-1}\widetilde{\alpha_p})}{\partial r}(t,r_1)P_L(t) - \widetilde{\alpha_p}(t,r_1)\frac{1}{2h}P_L(t)\right] \\ &-\frac{1}{6}\widetilde{\alpha_p}(t,r_1)\Big(\overline{Q_p}(r_1) + \overline{\mathbb{Z}}_p^T(r_1)\alpha^{(1)}(t)\Big)P_L(t) \\ &-\frac{1}{36}a_1\lambda(t)\Big[M_L(t)\big(P_L(t) + 4\alpha_1^{(1)}(t) + \alpha_2^{(1)}(t)\big) \\ &\qquad + P_L(t)\big(M_L(t) + 4\alpha_1^{(3)}(t) + \alpha_2^{(3)}(t)\big)\Big], \\ f_{N-1}(t,\boldsymbol{\alpha}(t)) = &-\frac{1}{6}\frac{d\alpha_N^{(1)}}{dt}(t) - \big(Q_p(r_{N-1}) + \mathbb{Z}_p^T(r_{N-1})\alpha^{(1)}(t)\big) \\ &\quad\times\left[\frac{1}{6r_{N-1}^{d-1}}\frac{\partial(r^{d-1}\widetilde{\alpha_p})}{\partial r}(t,r_{N-1})P_R + \widetilde{\alpha_p}(t,r_{N-1})\frac{1}{2h}P_R\right] \\ &-\frac{1}{6}\widetilde{\alpha_p}(t,r_{N-1})\Big(\overline{Q_p}(r_{N-1}) + \overline{\mathbb{Z}}_p^T(r_{N-1})\alpha^{(1)}(t)\Big)P_R \\ &-\frac{1}{36}a_1\lambda(t)\Big[M_R\big(P_R + 4\alpha_{N-1}^{(1)}(t) + \alpha_{N-2}^{(1)}(t)\big) \\ &\qquad + P_R\big(M_R + 4\alpha_{N-1}^{(3)}(t) + \alpha_{N-2}^{(3)}(t)\big)\Big], \\ f_N(t,\boldsymbol{\alpha}(t)) = &-\frac{1}{6}\frac{d\alpha_0^{(2)}}{dt}(t) - \big(Q_s(r_1) + \mathbb{Z}_s^T(r_1)\alpha^{(2)}(t)\big) \\ &\quad\times\left[\frac{1}{6r_1^{d-1}}\frac{\partial(r^{d-1}\widetilde{\alpha_s})}{\partial r}(t,r_1)S_L(t) - \widetilde{\alpha_s}(t,r_1)\frac{1}{2h}S_L(t)\right] \\ &-\frac{1}{6}\widetilde{\alpha_s}(t,r_1)\Big(\overline{Q_s}(r_1) + \overline{\mathbb{Z}}_s^T(r_1)\alpha^{(2)}(t)\Big)S_L(t) \\ &-\frac{1}{36}a_2\lambda(t)\Big[M_L(t)\big(S_L(t) + 4\alpha_1^{(2)}(t) + \alpha_2^{(2)}(t)\big) \\ &\qquad + S_L(t)\big(M_L(t) + 4\alpha_1^{(3)}(t) + \alpha_2^{(3)}(t)\big)\Big], \\ f_{2N-2}(t,\boldsymbol{\alpha}(t)) = &-\frac{1}{6}\frac{d\alpha_N^{(2)}}{dt}(t) - \big(Q_s(r_{N-1}) + \mathbb{Z}_s^T(r_{N-1})\alpha^{(2)}(t)\big) \end{aligned}$$

ETNA
Kent State University and
Johann Radon Institute (RICAM)

$$\times \left[\frac{1}{6r_{N-1}^{d-1}}\frac{\partial(r^{d-1}\widetilde{\alpha_s})}{\partial r}(t,r_{N-1})S_R + \widetilde{\alpha_s}(t,r_{N-1})\frac{1}{2h}S_R\right]$$
$$- \frac{1}{6}\widetilde{\alpha_s}(t,r_{N-1})\Big(\overline{Q_s}(r_{N-1}) + \overline{\mathbb{Z}}_s^T(r_{N-1})\alpha^{(2)}(t)\Big)S_R$$
$$- \frac{1}{36}a_2\lambda(t)\Big[M_R\big(S_R + 4\alpha_{N-1}^{(2)}(t) + \alpha_{N-2}^{(2)}(t)\big) + S_R\big(M_R + 4\alpha_{N-1}^{(3)}(t) + \alpha_{N-2}^{(3)}(t)\big)\Big],$$

$$f_{2N-1}(t,\boldsymbol{\alpha}(t)) = -\frac{1}{6}\frac{d\alpha_0^{(3)}}{dt}(t) + D\left(\frac{1}{h^2}M_L(t) - \frac{d-1}{2rh}M_L(t)\right) + \frac{M_s}{6}S_L(t)$$
$$- \frac{M_s}{36}\Big[M_L(t)\big(S_L(t) + 4\alpha_1^{(2)}(t) + \alpha_2^{(2)}(t)\big) + S_L(t)\big(M_L(t) + 4\alpha_1^{(3)}(t) + \alpha_2^{(3)}(t)\big)\Big]$$
$$- \frac{\eta}{36}\Big[M_L\big(P_L(t) + 4\alpha_1^{(1)}(t) + \alpha_2^{(1)}(t)\big) + P_L(t)\big(M_L(t) + 4\alpha_1^{(3)}(t) + \alpha_2^{(3)}(t)\big)\Big],$$

$$f_{3N-3}(t,\boldsymbol{\alpha}(t)) = -\frac{1}{6}\frac{d\alpha_0^{(3)}}{dt}(t) + D\left(\frac{1}{h^2}M_R + \frac{d-1}{2rh}M_R\right) + \frac{M_s}{6}S_R$$
$$- \frac{M_s}{36}\Big[M_R\big(S_R + 4\alpha_{N-1}^{(2)}(t) + \alpha_{N-2}^{(2)}(t)\big) + S_R\big(M_L(t) + 4\alpha_{N-1}^{(3)}(t) + \alpha_{N-2}^{(3)}(t)\big)\Big]$$
$$- \frac{\eta}{36}\Big[M_R\big(P_L(t) + 4\alpha_{N-1}^{(1)}(t) + \alpha_{N-2}^{(1)}(t)\big) + P_R\big(M_R + 4\alpha_{N-1}^{(3)}(t) + \alpha_{N-2}^{(3)}(t)\big)\Big],$$

with $f_j(t,\boldsymbol{\alpha}(t)) = 0$ for all $j \notin \{1, N-1, N, 2N-2, 2N-1, 3N-3\}$.

The solution of the ODE (5.11) can be approached using several methods found in the literature. However, due to the stiffness of the equation, which is a common characteristic in systems derived from discretized PDEs, common explicit methods, such as the popular Runge–Kutta family of integrators, are not suitable for such stiff problems. To overcome this limitation, we employ the BDF method, which is an implicit multi-step method specifically designed for solving stiff ODEs [18]. This method allows for larger time steps while maintaining accuracy and stability, which can be done by using information from previous time steps and solving an implicit equation at each step. Here, we apply the BDF method of order $p = 6$, for maximal stability and efficiency. The method applied to (5.11) gives the following approximations:

$$\mathbb{A}\alpha_n - \beta\Delta t\,\Phi(t_n,\alpha_n) - \mathbb{A}\sum_{j=0}^{p-1}\eta_j\alpha_{n-j-1} = 0. \tag{5.12}$$

In this context, $\Delta t = T/p$ represents the time step, and $\alpha_n = [\alpha_1^n, \ldots, \alpha_{N-1}^n]^T$ is the BDF method's approximation of the vector $\alpha(t)$ at time $t_n = n\Delta t$, for $n = 0, \ldots, p$. The coefficients η_j and β for the p-step BDF formula are provided in Table 5.2.

ETNA
Kent State University and
Johann Radon Institute (RICAM)

TABLE 5.2
BDF coefficients for order 6.

p	β	η_0	η_1	η_2	η_3	η_4	η_5
1	1	1					
2	$\frac{2}{3}$	$\frac{4}{3}$	$-\frac{1}{3}$				
3	$\frac{6}{11}$	$\frac{18}{11}$	$-\frac{9}{11}$	$\frac{2}{11}$			
4	$\frac{12}{25}$	$\frac{48}{25}$	$-\frac{36}{25}$	$\frac{16}{25}$	$-\frac{3}{25}$		
5	$\frac{60}{137}$	$\frac{300}{137}$	$-\frac{300}{137}$	$\frac{200}{137}$	$-\frac{75}{137}$	$\frac{12}{137}$	
6	$\frac{60}{147}$	$\frac{360}{147}$	$-\frac{450}{147}$	$\frac{400}{147}$	$-\frac{225}{147}$	$\frac{72}{147}$	$-\frac{10}{147}$

At each time step n, equation (5.12) for α_n must be solved by reformulating it into the following form:

$$\varphi(\alpha_n) = \mathbb{A}\alpha_n - \beta\Delta t\,\Phi(t_n, \alpha_n) - \mathbb{A}\sum_{j=0}^{p-1} \eta_j \alpha_{n-j-1} = 0.$$

To solve equation (5.12) for α_n efficiently, we employ the Newton method. We use the solution from the previous time step as an initial guess. The Newton method approximates α_n through a series of iterations (ζ_k) by

$$\begin{cases} \zeta_0, \\ \zeta_{k+1} = \zeta_k - [J_\varphi(\zeta_k)]^{-1}\varphi(\zeta_k), \quad k \geqslant 0. \end{cases}$$

Here $J_\varphi(\zeta_k)$ is the Jacobian matrix of φ, expressed as

$$J_\varphi(\zeta_k) = \mathbb{A} - \beta\Delta t\, J_\Phi(\zeta_k),$$

with J_Φ the Jacobian matrix of Φ with respect to α_n.

6. Numerical experiments. In this section, we aim to examine the accuracy of our proposed numerical scheme by comparing it with a known analytical solution. This evaluation is essential to determine the efficiency and validity of the method. The construction of a classical solution for a simplified version of the system in (4.1) presents significant challenges, mainly due to the nonlocal term, which must be calculated analytically in order to prevent errors that could arise from numerical integration. Then in Section 6.2, we use values similar to those reported by Lefebvre et al. [27], examining the dynamics of avascular tumor growth in the absence of medical treatment, considering a nonlocal velocity.

Throughout this section, we consider the spatial dimension of our system (2.2) to be $d = 2$. In this context, the nonlocal terms are expressed as

$$\begin{aligned} \mathbb{Z}_i^k(r) &:= (\widetilde{\gamma_k} \,\widetilde{*}\, B_i)(r) \\ &= 2\int_0^R \int_0^\pi \widetilde{\gamma_k}\Big(\sqrt{s^2 + r^2 + 2rs\cos(\theta)}\Big) B(s)s\,ds\,d\theta \end{aligned}$$

and

$$\begin{aligned} \overline{\mathbb{Z}}_i^k(r) &:= \frac{\partial(\widetilde{\gamma_k} \,\widetilde{*}\, B_i)(r)}{\partial r} \\ &= 2\int_0^R \int_0^\pi \frac{r + s\cos(\theta)}{\sqrt{r^2 + s^2 + 2rs\cos(\theta)}} \widetilde{\gamma_k}'\Big(\sqrt{s^2 + r^2 + 2rs\cos(\theta)}\Big) B(s)s\,ds\,d\theta. \end{aligned}$$

ETNA
Kent State University and
Johann Radon Institute (RICAM)

These double integrals are calculated numerically using the function `integral2` in MATLAB, which is effective for this type of two-dimensional integration over rectangular regions.

The simulations performed in Section 6.1 are executed in the spatial domain $[0, 1]$, while in Section 6.2, the spatial domain $[10^{-3}, 2]$ is considered. It is important to note that radial hyperbolic and radial parabolic equations are likely to suffer from singularities at the origin (see [30]). To mitigate this issue, the calculations are initiated from a small radius in space. The numerical simulations presented in this paper were performed using MATLAB on a standard laptop computer equipped with an Intel Core i5 processor (2.6 GHz, two cores) and 8 GB of RAM. No specialized GPU acceleration was utilized for these computations. This configuration was sufficient for running our simulations, demonstrating the efficiency of the proposed numerical method.

6.1. Convergence test with known analytical solution. In this section, we consider the following coupled system with source terms:

$$
\begin{cases}
\dfrac{\partial \widetilde{P}}{\partial t} + 2\pi r \dfrac{\partial}{\partial r}\left[\left(\displaystyle\int_0^R \widetilde{P}(t,s)s\,ds\right)\widetilde{P}\right] \\
\qquad\qquad = \left[H(\widetilde{M}) - t\widetilde{M} - 2\displaystyle\int_0^R \widetilde{P}(t,s)s\,ds\right]\widetilde{P} + f_1(t,r), \\
\dfrac{\partial \widetilde{S}}{\partial t} + 2\pi r \dfrac{\partial}{\partial r}\left[\left(\displaystyle\int_0^R \widetilde{S}(t,s)s\,ds\right)\widetilde{S}\right] \\
\qquad\qquad = -\left[t\widetilde{M} + 2\displaystyle\int_0^R \widetilde{S}(t,s)s\,ds\right]\widetilde{S} + f_2(t,r), \\
\dfrac{\partial \widetilde{M}}{\partial t} - 0.01\left(r\dfrac{\partial^2 \widetilde{M}}{\partial r^2} + \dfrac{\partial \widetilde{M}}{\partial r}\right) \\
\qquad\qquad = \widetilde{S}(1-\widetilde{M}) - \widetilde{M}\widetilde{P} + f_3(t,r), \\
\widetilde{U}(t,R) = \widetilde{U}_{ex}(t,R), \quad \widetilde{U}(t,0) = \widetilde{U}_{ex}(t,0), \quad t \in [0,T], \\
\widetilde{U}(0,r) = \widetilde{U}_{ex}(0,r), \quad r \in [0,R].
\end{cases}
\tag{6.1}
$$

The source term $(f(t,r) = f_1(t,r), f_2(t,r), f_3(t,r))$ is chosen in order that the system (6.1) has the analytical solution

$$
\begin{aligned}
\widetilde{U}_{ex}(t,r) &= \begin{bmatrix} \widetilde{P}_{ex}(t,r) \\ \widetilde{S}_{ex}(t,r) \\ \widetilde{M}_{ex}(t,r) \end{bmatrix} \\
&= \begin{bmatrix}
\dfrac{3}{2}\exp\left(\dfrac{\left(r-\frac{t}{2000}\right)^2}{50}\right) + \exp\left(\dfrac{\left(r-\frac{t}{350}\right)^2}{100}\right) + \dfrac{1}{2}\exp\left(\dfrac{\left(r-\frac{t}{400}\right)^2}{150}\right) \\
\dfrac{3}{2}\exp\left(\dfrac{\left(r-\frac{t}{2000}\right)^2}{70}\right) + \exp\left(\dfrac{\left(r-\frac{t}{350}\right)^2}{140}\right) + \dfrac{1}{2}\exp\left(\dfrac{\left(r-\frac{t}{400}\right)^2}{210}\right) \\
\dfrac{3}{2}\exp\left(\dfrac{\left(r-\frac{t}{2000}\right)^2}{80}\right) + \dfrac{4}{5}\exp\left(\dfrac{\left(r-\frac{t}{200}\right)^2}{160}\right) + \dfrac{3}{5}\exp\left(\dfrac{\left(r-\frac{t}{300}\right)^2}{240}\right)
\end{bmatrix}.
\end{aligned}
$$

ETNA
Kent State University and
Johann Radon Institute (RICAM)

The nonlocal system (6.1) can be considered a particular case of the general system (4.1) by setting specific parameter values. Specifically, we choose $\widetilde{\alpha_p}(t,r) = \widetilde{\alpha_s}(t,r) = r$, $\widetilde{\gamma_p}(r) = \widetilde{\gamma_s}(r) = 1$, $a_1 = 1$, $a_2 = 1$, $\lambda(t) = t$, $M_s = \eta = 1$, and $D = 0.01$. These parameters were selected to allow the radial convolution to be calculated analytically. This is important because radial systems often exhibit singularities at $r = 0$. To address these singularities, the velocity functions $\widetilde{\alpha_p}$ and $\widetilde{\alpha_s}$ and the diffusion parameter D are specially chosen.

To numerically solve the system, we discretize the domain $[0, R]$ using a uniform grid. The grid points are defined as $r_i = ih$, for $i = 1, \ldots, N$, where h is the spatial step size given by $h = R/N$, and N is the number of discretization nodes. We then compare the approximate numerical solution to the analytical solution using the relative error metrics defined as

$$E_n^{\infty} = \frac{\left\|\widetilde{U}(t^n) - \widetilde{U_h}(t^n)\right\|_{\infty}}{\left\|\widetilde{U}(t^n)\right\|_{\infty}} = \frac{\sup_{0\le i\le N}\left\|\widetilde{U}(t^n, r_i) - \widetilde{U_h}(t^n, r_i)\right\|}{\sup_{0\le i\le N}\left\|\widetilde{U}(t^n, r_i)\right\|}$$

and

$$E^{\infty} = \frac{\left\|\widetilde{U} - \widetilde{U_h}\right\|_{\infty}}{\left\|\widetilde{U}\right\|_{\infty}} = \frac{\sup_n \left\|\widetilde{U}(t^n) - \widetilde{U_h}(t^n)\right\|_{\infty}}{\sup_n \left\|\widetilde{U}(t^n)\right\|_{\infty}}.$$

Table 6.1 presents the execution times and relative errors for different numbers of nodes. Figure 6.1 illustrates the comparison between the approximate numerical solution, denoted as $\widetilde{U}_h$, and the exact solution, denoted as $\widetilde{U}_{ex}$, of our nonlocal system for a range of time values: $t = 0,\ t = 25,\ t = 50,\ t = 75$, and $t = 100$. Figures 6.2–6.4 provides illustrations of the approximate solutions.

TABLE 6.1
Execution time (seconds) and relative error for different node numbers for $R = 1$ and $T = 10$.

N	50	100	150	200	250	300
E^{∞}	3.344e-03	1.456e-03	6.610e-04	3.707e-04	2.440e-04	1.649e-04
CPU time	18.96	48.56	188.53	422.28	853.93	1619.54

In Figure 6.1, it is evident that the numerical solution approximates the exact solution with high accuracy across the different time instances ($t = 0,\ t = 25,\ t = 50,\ t = 75,\ t = 100$). This demonstrates the effectiveness of the numerical method over the specified time intervals.

Table 6.2 presents various values of the relative error E_n^{∞} for $\Delta t = h/2$ with different spatial step sizes h. The data suggest that, as h decreases, the computational error also decreases.

Figure 6.5a illustrates the decrease of the relative error E_{∞} as the number of grid points N increases from 100 to 500, while Figure 6.5b presents the convergence analysis in a log-log scale. The convergence order p is calculated as the slope of the best-fit line in logarithmic space, yielding $p \approx 1.98$. This value confirms second-order spatial accuracy, which is the expected theoretical convergence rate for cubic B-spline approximations.

Although proving the theoretical convergence of the BDF method for a nonlinear ODE is challenging, the computed results indicate a reduction in error with smaller spatial steps. This observation is consistent with existing literature on the numerical analysis and the stability of numerical integration methods. The known stability of the BDF method in stiff problems corroborates the observed error reduction trends with decreasing h-values.

ETNA
Kent State University and
Johann Radon Institute (RICAM)

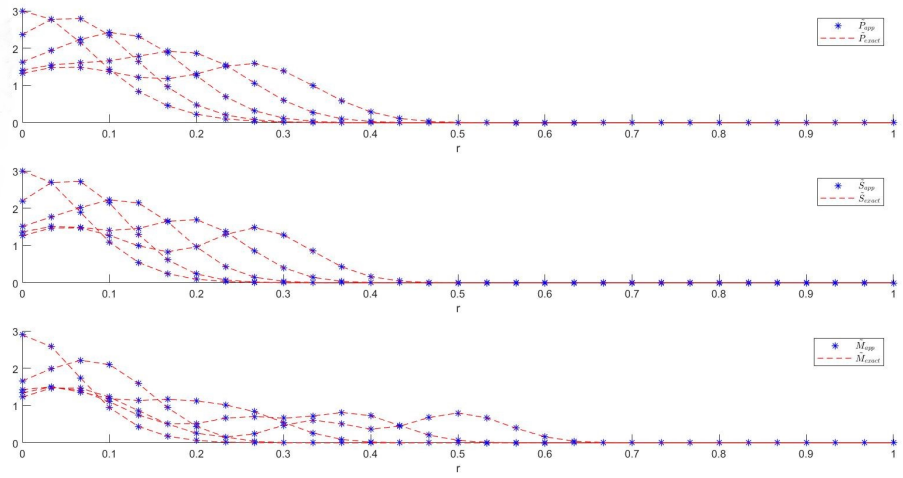

FIG. 6.1. *Approximate solution* $\widetilde{U}_h$ *and exact solution* $\widetilde{U}_{ex}$ *for* $t = 0,\ t = 25,\ t = 50,\ t = 75,\ t = 100$.

TABLE 6.2
Relative error E^{∞}.

N	100	200	300	400	500
h	0.01	0.005	0.0033	0.0025	0.002
Δt	0.005	0.0025	0.00165	0.00125	0.001
$t = 20$	6.9801e-04	1.7519e-04	7.7218e-05	4.3550e-05	2.7949e-05
$t = 40$	4.1530e-04	1.0432e-04	5.3297e-05	2.6102e-05	1.67076e-05
$t = 60$	8.0758e-04	2.0209e-04	9.0763e-05	4.9907e-05	3.2346e-05
$t = 80$	1.4171e-03	3.5577e-04	1.5894e-04	8.9162e-05	5.6989e-05
$t = 100$	1.8271e-03	4.5819e-04	2.0402e-04	1.1462e-04	7.3364e-05
E^{∞}	5.0599e-04	1.2579e-04	7.0742e-05	3.1597e-05	2.0176e-05

6.2. Numerical test for tumor growth. In this section, we present numerical simulations of the nonlocal tumor growth model (2.1) under the scenario of no medical intervention. The initial conditions for our simulations are defined as

$$\widetilde{P}(0,r) = \frac{0.3e^2}{e^2 + e^{20r}}, \quad \widetilde{S}(0,r) = \frac{0.8e^2 + e^{20r}}{e^2 + e^{20r}}, \quad \widetilde{M}(0,r) = 1.$$

At the boundary radius R, the conditions are specified as

$$\widetilde{P}(t,R) = 0, \quad \widetilde{S}(t,R) = 1, \quad \widetilde{M}(t,R) = 1.$$

The velocities and kernel functions incorporated in our model are expressed as

$$\widetilde{\alpha_p}(t,r) = \frac{2e}{e + e^{10r}}, \qquad \widetilde{\alpha_s}(t,r) = \frac{0.2e^{7.5}}{e^{7.5} + e^{15r}},$$
$$\widetilde{\gamma_p}(r) = 0.2\exp\left(-\frac{r}{50}\right), \qquad \widetilde{\gamma_s}(r) = \frac{1}{100}\exp\left(-\frac{r}{150}\right).$$

We used a hypoxia threshold value of $M_{th} = 0.5$. The growth factor parameter κ is set at 0.02. The model also integrates a diffusion coefficient D of 0.8. Furthermore, the nutrient

ETNA
Kent State University and
Johann Radon Institute (RICAM)

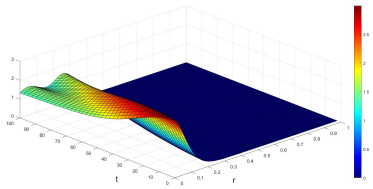

FIG. 6.2. *Approximation of* $\widetilde{P}$ *on* $[0,1] \times [0,100]$.

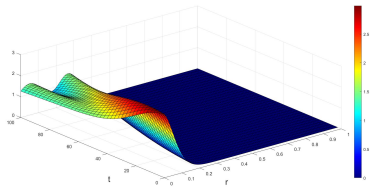

FIG. 6.3. *Approximation of* $\widetilde{S}$ *on* $[0,1] \times [0,100]$.

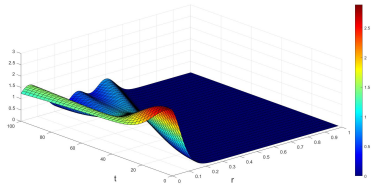

FIG. 6.4. *Approximation of* $\widetilde{M}$ *on* $[0,1] \times [0,100]$.

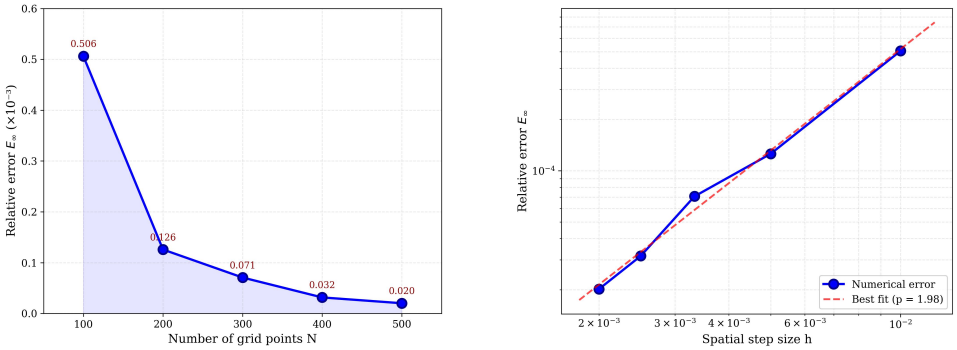

(a) Error decrease with mesh refinement.

(b) Convergence rate analysis.

FIG. 6.5. *Convergence analysis of the BDF B-spline collocation method for the nonlocal tumor growth model.*

consumption rate η is 1.5, and the blood vessel creation rate is characterized by $M_s = 1$. The results of our numerical simulations are shown in Figure 6.6.

Figures 6.7 and 6.8 illustrate the growth of the tumor core, particularly at its edges, where higher nutrient concentrations are present, facilitating cellular proliferation. The presence of abundant nutrients at the periphery enables the cells to rapidly divide and expand outward. In contrast, the center of the tumor exhibits a decrease in tumor cell density due to insufficient oxygen supply, leading to necrosis. The lack of oxygen, known as hypoxia, results in cell death and the formation of a necrotic core. This process highlights the dynamic nature of tumor growth, where peripheral areas continue to expand while central regions undergo cell death. Furthermore, the hypoxic conditions in the tumor center can lead to the release of signaling molecules that may promote angiogenesis or new blood vessel formation in an attempt to supply the tumor with more oxygen and nutrients.

7. Conclusion. The process of tumor growth remains a complex subject to study, predominantly due to the multifaceted nature of the factors that influence it. A detailed understanding

ETNA
Kent State University and
Johann Radon Institute (RICAM)

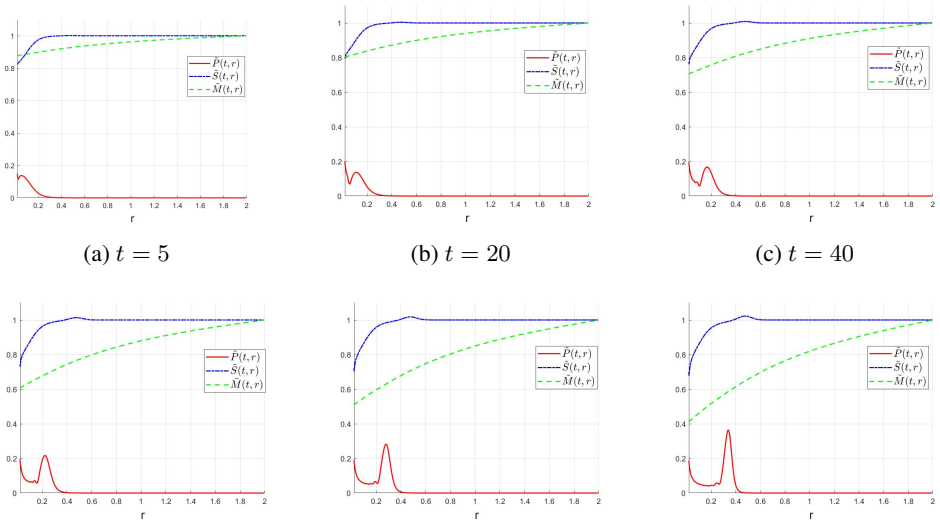

(a) $t = 5$ (b) $t = 20$ (c) $t = 40$

(d) $t = 60$ (e) $t = 80$ (f) $t = 100$

FIG. 6.6. *Radial tumor cells density $\widetilde{P}$, healthy cells density $\widetilde{S}$, and the concentration of nutriment and oxygen $\widetilde{M}$ for different time instants.*

of the mechanisms governing tumor growth is essential for the advancement of effective anticancer strategies.

In this paper, we have presented an innovative continuum model of tumor growth, which includes both cell-cell and cell-matrix adhesion and interactions. This model is characterized by the integration of nonlocal terms within a system of PDEs. We have successfully demonstrated the existence and uniqueness of solutions through the application of semigroup properties and Banach's fixed-point theorem, in combination with results established by Keimer et al. [25]. Furthermore, we have developed a numerical scheme for resolving the radial nonlocal system. This scheme employs B-splines for spatial discretization and the BDF method for temporal discretization. Extensive numerical tests have been conducted to validate the model's accuracy, and we have demonstrated experimental results related to tumor growth.

The use of nonlocal balance equations in our model offers several significant advantages over traditional local approaches. For example, nonlocal models can avoid the formation of shock waves and singularities that often challenge local hyperbolic systems. This regularizing effect leads to smoother solutions and may prevent the breakdown of numerical schemes, which is a common issue in local models of complex phenomena. The efficient numerical solution of nonlocal systems has potential applications in many fields such as population dynamics, material science, and climate modeling, where long-range effects play a crucial role and where avoiding discontinuities is critical.

In the future, our research aims to optimize the factors of medical drugs within the system (2.1), using the theory of optimal control for nonlocal balance equations. This may help in designing new strategies that minimize the auxiliary effects of treatment and maximize its efficacy. Using mathematical models, we intend to precisely adjust drug dosages, timings, and combinations to achieve the best therapeutic outcomes while reducing negative side effects.

ETNA
Kent State University and
Johann Radon Institute (RICAM)

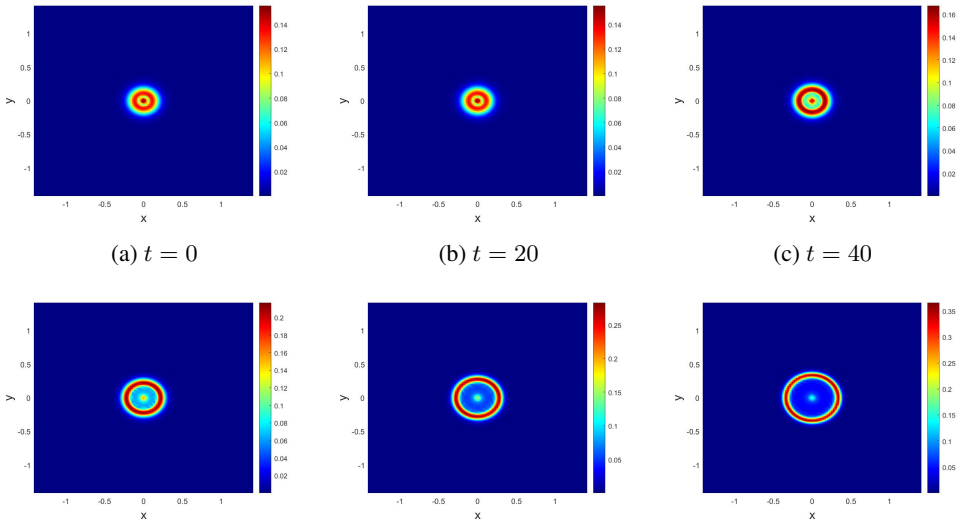

(a) $t = 0$ (b) $t = 20$ (c) $t = 40$

(d) $t = 60$ (e) $t = 80$ (f) $t = 100$

FIG. 6.7. *Tumor cells density P for different time instants.*

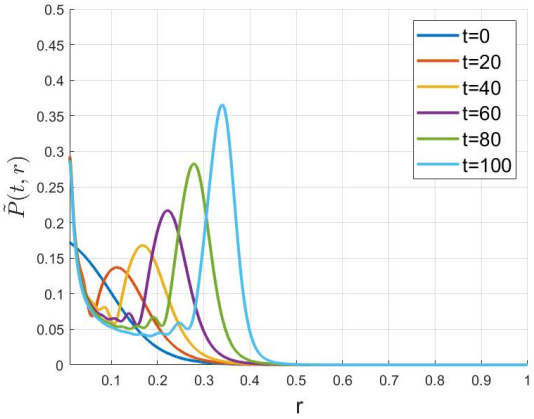

FIG. 6.8. *Radial tumor cells density for different time instants.*

Acknowledgment. The first author would like to thank the Centre National pour la Recherche Scientifique et Technique (CNRST) in Morocco and the Laboratoire de Mathématiques Pures et Appliquées (LMPA) at the Université du Littoral Côte d'Opale (ULCO) in France for their financial support. The authors would also like to thank the referees for their valuable remarks and suggestions, which have improved the quality of this paper.

REFERENCES

[1] I. ALI, M. YASEEN, AND I. AKRAM, *Utilizing cubic B-spline collocation technique for solving linear and nonlinear fractional integro–differential equations of Volterra and Fredholm types*, Fractal Fract., 8 (2024), Paper No. 268, 21 pages.

ETNA
Kent State University and
Johann Radon Institute (RICAM)

[2] N. J. ARMSTRONG, K. J. PAINTER, AND J. A. SHERRATT, *A continuum approach to modelling cell–cell adhesion*, J. Theoret. Biol., 243 (2006), pp. 98–113.
[3] S. BENZEKRY, C. LAMONT, D. BARBOLOSI, L. HLATKY, AND P. HAHNFELDT, *Mathematical modeling of tumor–tumor distant interactions supports a systemic control of tumor growth*, Cancer Res., 77 (2017), pp. 5183–5193.
[4] A. J. BERNOFF AND C. M. TOPAZ, *Biological aggregation driven by social and environmental factors: a nonlocal model and its degenerate Cahn–Hilliard approximation*, SIAM J. Appl. Dyn. Syst., 15 (2016), pp. 1528–1562.
[5] V. BITSOUNI AND R. EFTIMIE, *Non-local parabolic and hyperbolic models for cell polarisation in heterogeneous cancer cell populations*, Bull. Math. Biol., 80 (2018), pp. 2600–2632.
[6] H. BREZIS, *Functional Analysis, Sobolev Spaces and Partial Differential Equations*, Springer, New York, 2011.
[7] A. P. BROWNING, J. A. SHARP, R. J. MURPHY, G. GUNASINGH, B. LAWSON, K. BURRAGE, N. K. HAASS, AND M. J. SIMPSON, *Quantitative analysis of tumour spheroid structure*, eLife, 10 (2021), Paper No. e73020, 25 pages.
[8] H. BRUNNER, *Collocation Methods for Volterra Integral and Related Functional Differential Equations*, Cambridge University Press, Cambridge, 2004.
[9] A. BUTTENSCHÖN AND T. HILLEN, *Non-Local Cell Adhesion Models*, Springer, Cham, 2021.
[10] T. CAZENAVE AND A. HARAUX, *An Introduction to Semilinear Evolution Equations*, Oxford University Press, New York, 1998.
[11] W. CHEN, H. HUANG, R. HATORI, AND T. B. KORNBERG, *Essential basal cytonemes take up Hedgehog in the Drosophila wing imaginal disc*, Development, 144 (2017), pp. 3134–3144.
[12] C. DE BOOR, *A Practical Guide to Splines*, Springer, New York, 1978.
[13] Q. DU, *Nonlocal Modeling, Analysis, and Computation*, SIAM, Philadelphia, 2019.
[14] M. D'ELIA, Q. DU, C. GLUSA, M. GUNZBURGER, X. TIAN, AND Z. ZHOU, *Numerical methods for nonlocal and fractional models*, Acta Numer., 29 (2020), pp. 1–124.
[15] M. FRITZ, E. A. B. F. LIMA, V. NIKOLIĆ, J. T. ODEN, AND B. WOHLMUTH, *Local and nonlocal phase-field models of tumor growth and invasion due to ECM degradation*, Math. Models Methods Appl. Sci., 29 (2019), pp. 2433–2468.
[16] A. GERISCH AND M. CHAPLAIN, *Mathematical modelling of cancer cell invasion of tissue: local and non-local models and the effect of adhesion*, J. Theoret. Biol., 250 (2008), pp. 684–704.
[17] M. GHOLAMIAN AND J. SABERI-NADJAFI, *Cubic B-splines collocation method for a class of partial integro-differential equation*, Alexandria Eng. J., 57 (2018), pp. 2157–2165.
[18] E. HAIRER AND G. WANNER, *Solving Ordinary Differential Equations II*, Springer, Berlin, 1996.
[19] R. J. HANGELBROEK, H. G. KAPER, AND G. K. LEAF, *Collocation methods for integro-differential equations*, SIAM J. Numer. Anal., 14 (1977), pp. 377–390.
[20] Z. HEIDARY, S. HAGHJOOY JAVANMARD, I. IZADI, N. ZARE, AND J. GHAISARI, *Multiscale modeling of collective cell migration elucidates the mechanism underlying tumor–stromal interactions in different spatiotemporal scales*, Sci. Rep., 12 (2022), Paper No. 16242, 16 pages.
[21] T. HILLEN AND A. BUTTENSCHÖN, *Nonlocal adhesion models for microorganisms on bounded domains*, SIAM J. Appl. Math., 80 (2020), pp. 382–401.
[22] S. JAFARZADEH, F. MOUSAVI, A. LARIOS, AND F. BOBARU, *A general and fast convolution-based method for peridynamics: applications to elasticity and brittle fracture*, Comput. Methods Appl. Mech. Engrg., 392 (2022), Paper No. 114666, 36 pages.
[23] T. J. JEWELL, A. L. KRAUSE, P. K. MAINI, AND E. A. GAFFNEY, *Patterning of nonlocal transport models in biology: the impact of spatial dimension*, Math. Biosci., 366 (2023), Paper No. 109093, 16 pages.
[24] A. KEIMER AND L. PFLUG, *Existence, uniqueness and regularity results on nonlocal balance laws*, J. Differential Equations, 263 (2017), pp. 4023–4069.
[25] A. KEIMER, L. PFLUG, AND M. SPINOLA, *Existence, uniqueness and regularity of multi-dimensional nonlocal balance laws with damping*, J. Math. Anal. Appl., 466 (2018), pp. 18–55.
[26] L. A. KUNZ-SCHUGHART, M. KREUTZ, AND R. KNUECHEL, *Multicellular spheroids: a three-dimensional in vitro culture system to study tumour biology*, Int. J. Exp. Pathol., 79 (1998), pp. 1–23.
[27] G. LEFEBVRE, F. CORNELIS, P. CUMSILLE, T. COLIN, C. POIGNARD, AND O. SAUT, *Spatial modelling of tumour drug resistance: the case of GIST liver metastases*, Math. Med. Biol., 34 (2017), pp. 151–176.
[28] G. LORENZO, S. R. AHMED, D. A. HORMUTH, B. VAUGHN, J. KALPATHY-CRAMER, L. SOLORIO, T. E. YANKEELOV, AND H. GOMEZ, *Patient-specific, mechanistic models of tumor growth incorporating artificial intelligence and big data*, Ann. Rev. Biomed. Eng., 26 (2024), pp. 529–560.
[29] T. MICHEL, J. FEHRENBACH, V. LOBJOIS, J. LAURENT, A. GOMES, T. COLIN, AND C. POIGNARD, *Mathematical modeling of the proliferation gradient in multicellular tumor spheroids*, J. Theoret. Biol., 458 (2018), pp. 133–147.
[30] K. MOHSENI AND T. COLONIUS, *Numerical treatment of polar coordinate singularities*, J. Comput. Phys., 157 (2000), pp. 787–795.

ETNA
Kent State University and
Johann Radon Institute (RICAM)

[31] M. OSSWALD, E. JUNG, F. SAHM, G. SOLECKI, V. VENKATARAMANI, J. BLAES, S. WEIL, H. HORSTMANN, B. WIESTLER, M. SYED, ET AL., *Brain tumour cells interconnect to a functional and resistant network*, Nature, 528 (2015), pp. 93–98.

[32] A. RUSTOM, R. SAFFRICH, I. MARKOVIC, P. WALTHER, AND H.-H. GERDES, *Nanotubular highways for intercellular organelle transport*, Science, 303 (2004), pp. 1007–1010.

[33] D. STICHEL, A. M. MIDDLETON, B. F. MÜLLER, S. DEPNER, U. KLINGMÜLLER, K. BREUHAHN, AND F. MATTHÄUS, *An individual-based model for collective cancer cell migration explains speed dynamics and phenotype variability in response to growth factors*, npj Sys. Biol. Appl., 3 (2017), Paper No. 5, 10 pages.

[34] R. M. SUTHERLAND, J. A. MCCREDIE, AND W. R. INCH, *Growth of multicell spheroids in tissue culture as a model of nodular carcinomas*, J. Nat. Cancer Inst., 46 (1971), pp. 113–120.

[35] B. SZABÓ, G. J. SZÖLLÖSI, B. GÖNCI, Z. JURÁNYI, D. SELMECZI, AND T. VICSEK, *Phase transition in the collective migration of tissue cells: experiment and model*, Physical Rev. E, 74 (2006), Paper No. 061908, 5 pages.

[36] X. TIAN AND Q. DU, *Analysis and comparison of different approximations to nonlocal diffusion and linear peridynamic equations*, SIAM J. Numer. Anal., 51 (2013), pp. 3458–3482.

[37] S. ZHENG, *Nonlinear Evolution Equations*, Chapman and Hall/CRC, Boca Raton, 2004.